SYNTHESIS AND CHARACTERIZATION OF HYDROXYAPATITE-ALUMINA-ZIRCONIA BIOCOMPOSITES

A Thesis Submitted to the
Graduate School of Engineering and Sciences of
Izmir Institute of Technology
In Partial Fullfilment of the Requirements for the Degree of

MASTER OF SCIENCE

in Materials Science and Engineering

by
Erdem ŞAHİN

September 2006
İZMİR

ACKNOWLEDGEMENT

I would like to thank Prof. Dr. Muhsin Çiftçioğlu for his understanding, support and generosity in sharing his expertise.

I am thankful to all the colleagues who have made my life easier during the hard times of this work, to the Center for Materials Research staff for their tireless cooperation.

Finally I want to express my gratitude to my parents who made it possible to overcome all the obstacles I have come across throughout this work.

ABSTRACT

SYNTHESIS AND CHARACTERIZATION OF HYDROXYAPATITE-ALUMINA-ZIRCONIA BIOCOMPOSITES

Three component hydroxyapatite-alumina-zirconia composite presents a promising candidate material for bone replacement implants. Two methods were employed to synthesize the composite that is expected to have high bioactivity, high strength and high chemical stability in physiologic environment. Wet mixing and heterogeneous precipitation methods were used for the synthesis. Commercial hydroxyapatite, alum ina and yttria stabilized zirconia were mixed in varying proportions and obtained powders were sintered upto 1300 °C subsequent to dry pressing at 160MPa. An optimum composition of 10-20-70 volume percent zirconia, alumina and hydroxyapatite respectively was found to present the most suitable proportion in terms of sinterability and phase purity. β-tricalcium phosphate formation at temperatures higher than 1150 °C was found to be the only source of impurity phase in the material.

Heterogeneous precipitation method was applied to synthesize a composite material with a functionally graded structure. The three components were aimed to be coated on one another, zirconia (TZ-3Y) being the core, alumina being the intermediate layer and hydroxyapatite being the outer shell. The bulk composite was expected to have both enhanced mechanical properties and enhanced phase purity due to separation of two reactive phases, hydroxyapatite and zirconia by the alumina layer. The coating was done in two steps using urea as the precipitant, aluminum sulfate as the Al^{3+} source, calcium nitrate as the Ca^{2+} source and ammonium phosphate as the P source. Precipitation of aluminum hydroxides on TZ-3Y particulates and precipitation of calcium hydroxides as a nucleation point for hydroxyapatite on cores were facilitated through decomposition of urea above 85 °C in aqueous media. Particle size, distribution and morphology were monitored for alumina coated zirconia samples prepared with varying $Al_2(SO_4)$/Zirconia and urea/$Al_2(SO_4)$ molar ratios. The sample prepared with stoichiometric $Al_2(SO_4)$/Zirconia ratio and urea/$Al_2(SO_4)$ ratio 10 exhibited the most suitable composition and morphology for hydroxyapatite coating. Samples synthesized in the first step were used as cores for hydroxyapatite coating.

ÖZET

HİDROKSİAPATİT-ALUMİNA-ZİRKONYA BİOKOMPOZİTİNİN SENTEZİ VE KARAKTERİZASYONU

Üç bileşenli hidroksiapatit-alumina-zirkonya kompoziti kemik yerine geçen protezler için uygun bir malzeme sağlamaktadır. Vücutta yüksek biouyumluluk, mukavemet ve kimyasal kararlılık sergilemesi beklenen bu kompozit iki yöntem kullanılarak sentezlenmiştir. Sentezler ıslak karışım ve heterojen çökelme yöntemleri kullanılarak yapılmıştır. Ticari ayar hidroksiapatit, alumina ve itriya ile kararlılaştırılmış tetragonal zirkonya değişken oranlarda karıştırılmış ve elde edilen tozlar 160 MPa basınçla preslendikten sonra 1300 °C'ye kadar sinterlenmiştir. Hacimsel olarak yüzde 10-20-70 konsantrasyonundaki zirkonya, alumina ve hidroksiapatitin sinterlenebilme ve faz saflığı bakımından en uygun orandaki malzeme olduğu görülmüştür. 1150 °C üzeri sıcaklıklardaki beta-trikalsiyum fosfat oluşumu malzemedeki tek safsızlık kaynağı olarak bulunmuştur.

Heterojen çökelme yöntemi fonksiyonel özellikli yapıda bir kompozit malzeme sentezlemek için uygulanmıştır. Üç bileşenin zirkonya içte, alumina ara katmanda ve hidroksiapatit dışta olmak üzere birbirlerinin üzerine kaplanması hedeflenmiştir. Bu yapıya sahip kompozit kitlesinin sinterlendiğinde gelişmiş mekanik özelliklere ve alumina katmanının hidroksiapatit ve zirkonya fazlarını ayırıcı özelliğinden dolayı yüksek faz saflığına sahip olması beklenmektedir. Kaplamada, çökeltici olarak üre, Al^{3+} kaynağı olarak aluminum sulfat, Ca^{2+} kaynağı olarak kalsiyum nitrat ve P kaynağı olarak amonyum fosfat kullanılmıştır. Aluminyum hidroksitin zirkonya tanelerinin üstüne çökelmesi ve hidroksiapatit çekirdeklenme noktası olarak calcium hidroksitlerin alumina kaplanmış zirkonya tanelerinin üstüne çökelmesi, 85 °C üzerinde üre bozunması yoluyla sağlanmıştır. Değişken $Al_2(SO_4)$/Zirkonya ve üre/$Al_2(SO_4)$ molar oranlarıyla hazırlanmış alumina-zirkonya kompozitlerinin parçacık boyutu, dağılımı ve iç yapısı incelenmiştir. 1.6 $Al_2(SO_4)$/Zirkonya oranı ve 10 üre/$Al_2(SO_4)$ oranı ile hazırlanan örneğin hidroksiapatit kaplaması için en uygun kompozisyona ve morfolojiye sahip olduğu görülmüştür. İlk kademede sentezlenen örnekler hidroksiapatit kaplaması için çekirdek tane olarak kullanılmıştır.

TABLE OF CONTENTS

LIST OF FIGURES

LIST OF TABLES

CHAPTER 1

INTRODUCTION

Nowadays medical world is in a transition from curing damaged organs of the patient by lengthy surgical operations to replacing the damaged organ completely with in vitro synthesised implants. Artificial soft tissues and organs are products of the research on the growth of stem cells on bioactive scaffolds and will be commonly available soon following extensive biomedical research and development. Hard tissue and bone replacements are synthesised mainly from bioactive and strong materials with similar chemical and phase structure to the hard tissues. Research on synthesis of new biomaterials involves the use of the present biomaterials in a new composite material with enhanced properties, modification of the microstructure of the present biomaterials and chemical synthesis of new novel biomaterials. Material scientists are currently working on projects for the synthesis of biocompatible materials which mimic the properties of natural bone.

Bone graft is the second most common transplantation tissue, with blood being by far the commonest. More than 2.2 million bone grafting procedures are performed worldwide annually in order to repair bone defects in orthopaedics, neurosurgery and dentistry. Bone-grafting is usually required to stimulate bone-healing. Several methods of reconstructing defective bones are available namely using autograft, allograft, demineralised bone matrix, hydroxyapatite calcium phosphate, autologous bone marrow aspirates, bone morphogenetic proteins, and several other related growth factors.

The highest standard of bone-grafting is harvesting autologous cortical and cancellous bone from the iliac crest. All other forms of bone grafting have disadvantages compared to autograft and as such their use is sub-optimal. However, technological evolution along with better understanding of bone-healing biology have lead to the development of several bone graft substitutes that are currently available to the orthopaedic surgeons.

Bone tissue properties like having a relatively low weight, porous microstructure, viscoelasticity necessitates the use of materials as bone graft substitutes with lower weights which can be shaped precisely, and can gradually dissolve and be replaced by the natural bone tissue. Bioceramics are a class of materials that satisfy

most of these criteria in addition to their biocompatibility and sufficient mechanical strength close to that of bone.

Hydroxyapatite (HA) has been the focus of biomaterials research as a highly biocompatible ceramic with a relatively simple processing. Its use in orthopedic surgery and as bone graft substitute has dominated any other material in quantity. Biomaterials with improved mechanical properties have been synthesized by the incorporation of hydroxyapatite in composites as a ceramic matrix. HA has also been used to increase the biocompatibility of mechanically strong materials either as coating or reinforcement particles or fibers. The versatility of HA as part of biocomposites enables materials engineers to combine materials with various degrees of biocompatibility to produce satisfactory biomaterials for a certain application in the body.

The goal of this work was to synthesise a biocomposite composed of bioinert and tough zirconia toughened alumina and bioactive hydroxyapatite in the nanoscale by colloidal methods. The three component composite particulates having a narrow size distribution was aimed to be obtained by heterogeneous precipitation method and then to be sintered into a bulk ceramic composite having a morhological similarity to bone tissue with an expected mechanical strength higher than that of bone due to transformation toughening capability of yttria-stabilized zirconia core particulates.

Previous researchers have produced similar three component biocomposites by mixing hydroxyapatite with alumina coated zirconia and obtained better mechanical properties in samples prepared with coated particles compared to the ones prepared by mechanically mixing the three components (Kim et al. 1999). The improvement in homogeneity of the microstructure in the coated samples presents an advantage of this method.

The motivation behind this work was making use of individual coating of the ceramic submicron powder particles in aqueous medium, transformation toughening property of tetragonal zirconia polycrystals, tribologic advantages of alumina and bioactivity of hydroxyapatite in a bone-mimetic bioceramic. The synthesised composite may have a use as nanoscale ceramic particulates as coatings that have improved mechanical integrity or as dense or porous bulk ceramic for bone graft substitutions.

CHAPTER 2

BIOMATERIALS

Only a few of the materials known satisfy the requirements of implantation in the body. These biomaterials belong to all 5 major classes of materials: metals, ceramics, polymers, composites and natural materials. Wide diversity of these materials used in medicine is a result of materials research done in the last 50 years by controlling the composition, purity, physical properties of the materials and synthesizing new materials with new and special properties. These biomaterials are tailored according to the needs of medical devices such as woven polymer fibers in vascular grafts, bundles of cellulose acetate fibers in artificial kidney dialysers, and titanium alloys in hip replacements (Ratner et al. 2004).

The common property of all the biomaterials is biocompatibility or non-toxicity which is the definition of a material that is not recognized by the body as a potentially harmful foreign substance. Body can react instantly to a foreign material by the cells in body fluid and start an inflammation reaction followed by a wound healing process. Once an implant is placed in the body, an injury response is initiated by the tissue that results in inflammation as a reaction to local injury. Injury at the implant site leads to immediate development of the provisional matrix which consists of fibrin and inflammatory products released by the activated platelets, inflammatory cells and endothelial cells. Not all biocompatible materials are inert in the body but the highly bioactive ones incorporate to the actions of body like providing a host matrix for tissue growth or being slowly replaced by the growing tissue. Biocompatible materials are classified as bioinert, resorbable and bioactive according to tissue response. Bioinert materials induce formation of a fibrous tissue of variable thickness, interfacial bond forms on bioactive materials, and resorbable materials are replaced by the surrounding tissue (Ratner et al. 2004). Materials capable of evading attack by the body's immune system, and of stimulating tissue growth, are potentially far more effective and less costly.

Mechanical similarity of the biomaterial to the host or replaced tissue is another important property. Especially in hard tissue replacements the biomaterial is required to support or share a portion of the load. Compressive strength, fracture toughness and hardness of biomaterials are important in these cases. Table 1 gives a list of biomaterials used in body implants with their properties.

Table 1. Biomaterials and their properties.

Type	Properties	Applications
Polymers		
PMMA	High toughness, stability	Bone cement
	Excellent light transmittance	Intraocular lenses
PHEMA	Excellent light transmittance	Soft contact lenses
Polyacrylic acid	High adhesive strength	Dental cement
		Mucosal drug delivery
Polyethylene	High toughness, wear resistance	Catheters
		Acetabular component in artificial hips
Polypropylene	High tensile strength, chemical resistance	Sutures
		Hernia repair
PTFE	High hydrophobicity	Catheters
	Excellent lubricity	Vascular grafts
Poly(dimethyl siloxane)	Low T_g	Finger joints
	Low mechanical properties	Heart valves
	High flexibility	Breast implants
PET	High tensile strength	Arterial grafts
		Fixation of implants
Cellulose acetate	High absorbance	Dialysis membrane
Nylon	High chemical resistance	Surgical sutures
PLGA	Bioresorbable	Drug delivery systems
		Fixation devices
Polyurethane	High fatigue resistance	Pacemaker insulation
		Vascular grafts
Metals		
316L Stainless steel	High corrosion resistance	Bone screws
	High strength	Hip prostheses
Co-Cr-Mo F75	High corrosion resistance	Heart valve stents
	Low fatigue resistance	
Ti-6Al-4V	High strength	Heart housing
	High corrosion resistance	Heart valve stents
Ceramics		
Al_2O_3	High corrosion resistance	Hip prostheses
	High wear resistance	Dental implants
ZrO_2	Low modulus of elasticity	Articulating ball in
	High strength	total hip prostheses
Bioactive glasses	High strength	Orthopedic,
		Maxillofacial prosth
Hydroxyapatite	High bioactivity	Dental implants
	Low strength	Alveolar ridge
		Periodontal pocket
Calcium phosphates	High bioactivity	Degradable bone filler
Pyrolytic carbon	High Strength	Heart valves
	High wear resistance	Dental implants
Composites		
Hydroxyapatite-	High bioactivity	Bone implant
Polyethylene	High toughness	
Alumina-Zirconia	High wear resistance	Femoral heads
Natural Materials		
Chitosans		Wound dressing
Collagen		Soft tissue coatings
Gelatin		Artificial heartbladder
Hyaluronic acid		Urinary bladder
		Wound dressing

2.1. Bioceramics

Ceramics are a versatile group of materials that are abundant in type. Oxides are the most commonly used ceramics also found in great quantities in nature. The chemical synthesis, shaping and heat treatment processes of oxides are relatively simple compared to other materials. The properties common to all ceramics are chemical stability, low density, high hardness, low tensile strength and high compressive strength. Ceramics are ideal materials for mobile load bearing components in aggressive environments such as engine blocks, refractories and hard tissue replacements.

Body is an active system regularly maintaining itself with its defense mechanism for optimum working conditions. A continuous process of building up and breaking down biostructures provides a demanding aggressive environment for body components. The actions of living cells as a part of the immune system are on the nanoscale and are basically chemical dissolution and adsorption processes. Following contact with body tissue, bare surface of a biomaterial is covered rapidly with proteins that are adsorbed from the surrounding body fluids. The chemistry of the underlying substrate, due to its effect on wettability and surface charge, controls the nature of the adherent protein layer. Macrophage fusion and platelet adhesion are strongly dependent on surface chemistry. Although cells are able to adhere, spread and grow on bare biomaterial surfaces in vitro, proteins adsorbed from the adjacent tissue environment and adherent cells enhance cell attachment, migration and growth. Cell adhesion to biomaterials is mediated by cytoskeletally associated receptors in the cell membrane which interact with cell adhesion proteins that adsorb to the material surface from the surrounding plasma. The chemical nature of a biomaterial placed in the body as an implant therefore is important in functioning of the body. Some ceramics that have been tested in vivo do not cause increased activity of immune system when dissolved in body fluid or in contact with tissues. Such ceramics, mainly oxides, are termed bioceramics.

Bioceramics have the advantage of being compatible with the human body environment. Their biocompatibility is a direct result of their chemical compositions which contain ions commonly found in the physiological environment such as Ca^{2+}, K^{+}, Mg^{2+}, Na^{+}, and of other ions showing very limited toxicity to body tissues (such as Al^{3+} and Ti^{2+}). Due to their excellent tribological properties and with their improved fracture toughness and reliability, structural ceramics such as polycrystalline alumina and

toughened zirconia have been used as hard tissue replacement materials. One remarkable success of bioceramics as implant materials over the last two decades has been the emergence and clinical use of bioactive ceramics that elicit a specific biological response at the interface of the material resulting in the formation of a strong bond between the tissue and the material. These bioceramics include calcium phosphates with hydroxyapatite being the prominent family member, Bioglasss, A-W glass–ceramic, and other bioactive glasses and glass–ceramics (Wang et al. 2003). However, the brittle nature of ceramics such as alumina and the low strength of bioactive ceramics such as hydroxyapatite have limited their scope of clinical applications.

Bioceramics are generally used to repair or replace skeletal hard tissues and their stable attachment to connective tissue varies significantly. Bioceramics can be classified into four groups based on their type of attachment to the surrounding tissues. Dense and nearly inert ceramics attach to the bone by morphological fixation, or growth of bone into surface irregularities. Porous and inert ceramics are attached to the bone by ongrowth of the tissue or biological fixation. Dense and surface reactive ceramics attach directly by chemical bonding to the bone or bioactive fixation. Resorbable ceramics attach to the bone by any of the above mechanisms and are slowly replaced by bone. Examples to each of these types of bioceramics are Al_2O_3, HA coated porous implants, Hydroxyapatite, and Tricalcium phosphate respectively. A list of bioceramics used today is given in Table 2 (Ratner et al. 2004).

Table 2. Bioceramics and Their Applications.

Orthopedic load-bearing applications	**Coatings for tissue ingrowth (Cardiovascular, orthopaedic, dental and maxillofacial prosthetics)**
Al_2O_3 ZrO_2	Al_2O_3
Coatings for chemical bonding (Orthopaedic, dental and maxillofacial prosthetics)	**Temporary bone space fillers**
HA Bioactive glasses Bioactive glass-ceramics	Tricalcium phosphate Calcium and phosphate salts
Dental implants	**Periodontal pocket obliteration**
Al_2O_3 HA Bioactive glasses	HA HA-PLA composite Trisodium phosphate Calcium and phosphate salts Bioactive glasses
Alveolar ridge augmentations	**Maxillofacial reconstruction**
Al2O3 HA HA-autogenous bone composite HA-PLA composite Bioactive glasses	Al2O3 HA HA-PLA composite Bioactive glasses
Otolaryngological	**Percutaneous access devices**
Al_2O_3 HA Bioactive glasses Bioactive glass-ceramics	Bioactive glasses Bioactive composites
Artificial tendon and ligament	**Orthopaedic fixation devices**
PLA-carbon fiber composite	PLA-carbon fibers PLA-calcium/phosphorus-base glass fibers

2.2. Hydroxyapatite

The main crystalline component of the mineral phase of bone is calcium deficient carbonate-hydroxyapatite. Similarity of synthetic hydroxyapatite to bone mineral makes it the most clinically used biomaterial. Hydroxyapatite has a hexagonal symmetry and unit cell lattice parameters a = 0.95 nm and c = 0.68 nm. Taking into account the lattice parameters and its symmetry, its unit cell is considered to be arranged along the c-axis. This would justify a preferred orientation that gives rise to an oriented growth along the c-axis and a needle-like morphology.

Hydroxyapatite belongs to calcium phosphate class that is characteristically resorbable in body. Tetracalcium Phosphate ($Ca_4P_2O_9$), Amorphous calcium Phosphate, α-Tricalcium Phosphate ($Ca_3(PO_4)_2$), β-Tricalcium Phosphate ($Ca_3(PO_4)_2$) , and Hydroxyapatite ($Ca_{10}(PO_4)_6(OH)_2$) are members of calcium phosphates in order of decreasing solubility in body fluids. Unlike the other calcium phosphates, hydroxyapatite does not break down under physiological conditions. In fact, it is thermodynamically stable at physiological pH and actively takes part in bone bonding, forming strong chemical bonds with surrounding bone. For bone mimetic implants synthetic hydroxyapatite is produced by various methods.

Hydroxyapatite is a thermally unstable compound, decomposing at temperatures from about 800-1200°C depending on its stoichiometry. The stoichiometry of hydroxyapatite is highly significant if thermal processing of the material is required. Calcium phosphate phases of alpha and beta-tricalcium phosphate, tetracalcium phosphate occur with slight imbalances in the stoichiometric ratio of calcium and phosphorus in HA from the molar ratio of 1.67. It is also important to know the close relation between the stoichiometry, acidity and solubility. Thus, it is known that the lower the Ca/P ratio and the larger the acidity of the environment, the higher will be the solubility of the HA. For Ca:P < 1, both acidity and solubility are extremely high, and both parameters decrease substantially for Ca/P ratios close to 1.67, which is the value of stoichiometric hydroxyapatite. A list of calcium phosphate phases arranged according to their Ca/P ratio is given in Table 3 (Vallet-Regi et al. 2004). The prevention of the formation of calcium phosphate phases with relatively higher solubility is significant when stability of hydroxyapatite is an important issue in the application. It is possible to

sinter phase pure hydroxyapatite using stoichiometric composition at temperatures up to 1300 °C.

Hydroxyapatite lacks the mechanical strength required for long term use in biomedical implants. In practice hydroxyapatite is either used as a bioactive coating on implants or reinforced by metal or ceramic phases. Many reinforcements, including particles, platelets, whiskers, long fibers, partially stabilized zirconia (PSZ), metal dispersoids, and nanoparticles have been used in HA ceramics to improve their reliability. The highest values of fracture toughness(K_{Ic}) and fracture strength(σ_f) for HA based materials were reported for HA matrix composites containing 20–30% Fe-Cr alloy long metal fibers (K_{Ic} - 6.0–7.4 MPa/m$^{1/2}$, σ_f -175–224 MPa) (Suchanek et al. 1997). The biocompatibility of the metal-reinforced HA composites will be significantly inferior compared to pure HA. In the case of other HA-based composites K_{Ic} was found in the range of 1.4–3.9 MPa/m$^{1/2}$, depending upon used reinforcement. Typical mechanical properties of dense hydroxyapatite are given in Table 4 (Silva et al. 2000).

Several techniques have been utilized for the preparation of hydroxyapatite. Materials with various morphology, stoichiometry, and level of crystallinity have been obtained depending on the technique. The synthetic routes employed can be divided into solid-state reactions and wet methods, which include precipitation, hydrothermal and hydrolysis of other calcium phosphates. Modifications of these “classical” methods (precipitation, hydrolysis or precipitation in the presence of urea) or alternative techniques have been employed to prepare hydroxyapatite with morphology, stoichiometry, ion substitution or degree of crystallinity as required for a specific application. Sol–gel, microwave irradiation, freeze drying, mechanochemical method, emulsion processing, spray pyrolysis, hydrolysis of a-TCP can be listed as some of these techniques (Vallet-Regi et al. 2004) A stoichiometric and well crystallized product with low sinterability is obtained with wet methods but relatively high temperatures and long heat treatment times are required in synthesis. Nanometer sized crystals can be obtained at temperatures lower than 100 °C with precipitation techniques in the shape of needles, rods or equiaxed particles (Aizawa et al., 1998). Their crystallinity and stochiometry is close to well crystallized stoichiometric HA under precise control of preparation conditions. A common method of precipitation synthesis of HA is by using calcium nitrate and ammonium phosphate in the presence of ammonium hydroxide (Mobasherpour et al. 2006). A basic medium favors HA precipitation by the following reaction:

$10Ca(NO_3)2{\cdot}4H_2O + 6(NH_4)_2HPO_4 + 8NH_4OH \rightarrow Ca_{10}(PO_4)_6(OH)_2 + 20NH_4NO_3 + 20H_2O$ (1)

Hydrothermal techniques give hydroxyapatite powders with a high degree of crystallinity and better stoichiometry having a wide distribution of crystal sizes.

Applications of hydroxyapatite include surface coating of orthopedic and dental metal implants where HA both promote osseointegration process and reduce metal ion release by acting as a physical barrier; bioceramic preparation for replacements of bone fragments, repair of periodontal bony defects; and use as drug carrier for controlled drug release with promising potential to heal bone fractions and suppress inflammation process. Hydroxyapatite has been used clinically in different applications. It has been utilized as a dense, sintered ceramic for middle ear implants, alveolar ridge reconstruction and augmentation, in porous form as granules for filling body defects in dental and orthopaedic surgery and as a coating on metal implants (Lazic et al. 2001).

Table 3. Various calcium phosphates with their respective Ca/P ratios

Ca/P	Name	Formula	Acronym
2,0	Tetracalcium phosphate	$Ca_4O(PO_4)_2$	TetCP
1,67	Hydroxyapatite	$Ca_{10}O(PO_4)_6(OH)_2$	HA
1,50	Tricalcium phosphate	$Ca_3(PO_4)_2$	TCP
1,33	Octacalcium phosphate	$Ca_8H_2(PO_4)_6{\cdot}5H_2O$	OCP
1,0	Dicalcium phosphate dihydrate	$CaHPO_4{\cdot}2H_2O$	DCPD
1,0	Dicalcium phosphate	$CaHPO_4$	DCPA
1,0	Calcium pyrophosphate	$Ca_2P_2O_7$	CPP
1,0	Calcium pyrophosphate dihydrate	$Ca_2P_2O_7{\cdot}2H_2O$	CPPD
0,7	Heptacalcium phosphate	$Ca_7(P_5O_{16})_2$	HCP
0,67	Tetracalcium dihydrogen phosphate	$Ca_4H_2P_6O_{20}$	TDHP
0,5	Monocalcium phosphate monohydrate	$Ca(H_2PO_4)_2{\cdot}H_2O$	MCPM
0,5	Calcium metaphosphate	$Ca(PO_3)_2$	CMP

Table 4. Typical Mechanical Properties of Dense Hydroxyapatite Ceramics

Theoretical density	3.156 g/cm^3
Hardness	500-800 Vickers, 2000-3500 Knoop
Tensile strength	40-100 MPa
Bend strength	20-80 MPa
Compressive strength	100-900 MPa
Fracture toughness	approx. 1 MPa/m$^{1/2}$
Young's modulus	70-120 GPa

2.3. Alumina

Biocompatible ceramics with mechanical properties comparable to metals are preferred in parts of the body that have high wear risk. An inert ceramic, alumina is used in load bearing hip prosthesis and dental implants in dense and pure state because of its excellent corrosion resistance, high strength and high wear resistance. Alumina's long term use in orthopedic surgery has been motivated by its excellent biocompatibility and very thin capsule formation which permits cementless fixation of prostheses as well as its very low coefficients of friction and wear. The exceptional tribologic properties of alumina are due to small grain sizes less than 4 microns and narrow grain size distribution which lead to very low surface roughness. Rapid wear of bearing surfaces takes place in the case of large grain presence owing to grain pull out due to local dry friction.

As a mechanically strong ceramic alumina is also used as a reinforcing material in biocomposites. Strength, fatigue resistance and fracture toughness of polycrystalline alpha alumina are functions of grain size and purity. Good flexural strength, excellent resistance to dynamic and impact fatigue, resistance to subcritical crack growth and excellent compressive strength are obtained with average grain sizes < 4 microns and purity >99.7%.(Ratner et al. 2004) Mechanical properties of alumina used in implants are listed in Table 5. Clinical applications of alumina include knee prostheses, bone and dental screws, alveolar ridge and maxillofacial reconstruction, ossicular bone substitutes, corneal replacements and segmental bone replacements.

Table 5. Mechanical properties of biomedical grade alumina

Density	3.97 g/cm^3 (99.9% Al_2O_3)
Hardness	2200 Vickers
Bend strength	500 MPa
Compressive strength	4100 MPa
Fracture toughness	4 MPa/m$^{1/2}$
Young's modulus	380 GPa
Thermal expansion coefficient	8x10^{-6} 1/K

2.4. Zirconia

Zirconia is an inert ceramic in its pure form which possesses extraordinary properties when doped with certain stabilizing oxides such as yttria, magnesia and calcia. It is a well-known polymorph that occurs in three forms: monoclinic (M), tetragonal (T), and cubic (C). Pure zirconia is monoclinic at room temperature. This phase is stable up to 1170°C. Above this temperature it transforms into tetragonal and then into cubic phase at 2370°C. During cooling, a T→M transformation takes place in a temperature range of about 100°C below 1070°C. The improved mechanical properties due to transformation toughening of tetragonal zirconia is utilized in biocomposites as well as conventional ceramic applications because of its good biocompatibility. The properties of interest to the engineer utilizing zirconia ceramics include strength, toughness, hardness, wear resistance and thermal properties.

The type and amount of additives to stabilize zirconia in its tetragonal crystal structure is the important variable in composition that affects all of the mechanical properties. The yttria content is the most significant controlling variable in yttria-stabilized zirconia ceramics. In order to improve the mechanical properties it is essential to have a microstructure free of any monoclinic phase which would act as a flaw, and this dictates the minimum level of stabiliser added. Approximately 1.8 mol% yttria in solid solution results in a ceramic with a composition close to the phase boundary where the metastable tetragonal phase is transformable. As a consequence high values of fracture toughness can be obtained with this composition. A maximum in the fracture strength is obtained at the 3 mol % yttria composition in research done so far.

Tetragonal zirconia experiences a degradation when in contact with water at temperatures in the 200-300 °C range due to ageing of the metastable phase which restricts its use in long term applications (Stevens et al. 1986).

Biomedical grade zirconia exhibits the best mechanical properties of oxide ceramics. Today, more than 600 000 zirconia femoral heads have been implanted in joint replacement operations worldwide. The mechanical properties of commercial yttria stabilized zirconia is given in Table 6 (Piconi et al. 1997).

Table 6. Mechanical properties of zirconia TZ-3Y

Density	6.05 g/cm^3
Hardness	1200 HV
Bend strength	900-1200 MPa
Compressive strength	2000 MPa
Fracture toughness	7-10 MPa/m$^{1/2}$
Young's modulus	210 GPa
Thermal expansion coefficient	11x10^{-6} 1/K

2.5. Hard Tissue Replacement

A high impact load on a part of the skeletal system usually results in a fracture or crack on the hard tissue and necessitates medical treatment to heal or replace the damaged hard tissue. Long term degenerative diseases cause similar effects on the hard tissues by excessive wear or local corrosion of the hard tissues. The common hard tissue injuries include active parts of the body such as dental parts, trabecular bones, and hip joints. While some of these injuries are not so serious as to necessitate surgical operations, some hard tissue injuries require in vivo medical treatment and replacement of the damaged part. All attempts to synthesize bone replacement materials for clinical applications featuring physiological tolerance, biocompatibility and long term stability have, up to now, had only relative success; it comes to show the superiority and complexity of the natural structure where, for instance, human femur can withstand loads of up to 1650 kg (Vallet-Regi 2004).

Of all the joints, the hip and knee are the most important joints in a human body. The hip joint consists of two complementary articular surfaces separated by articular cartilage and the synovial fluid that has a pH between 7.29 and 7.45. Excessive wear of the interfaces due to a degenerative disease such as osteoarthritis or injury requires a replacement of the entire hip joint. In a hip joint the head of the femoral element fits inside the cup to enable the articulation. These two parts of the hip implant have been made using a variety of materials such as metals, ceramics, polymers and composites (Katti et al. 2004). Typical polymeric materials alone tend to be too weak to be suitable for total hip replacement components that should fulfill requirement of stress deformation responses. Metals typically have good mechanical properties but show poor biocompatibility, cause stress shielding and release of dangerous metal ions causing eventual failure and removal of implant. Ceramics generally have good biocompatibility but poor fracture toughness and tend to be brittle. Composite materials with engineered interfaces resulting in combination of biocompatibility, mechanical strength and toughness, is the focus of extensive research and this study.

One of the major problems materials science and engineers working on the improvement of current implant materials is the fact that these biomaterials are generally much stiffer than the human cortical bone. According to the load sharing principle of the composite theory, if a stiff metal or ceramic implant is placed in the bone, the bone will be subjected to lower mechanical stresses, and consequently bone will resorb. This is known as "Wolff's Law", i.e., with the changing stress or strain imposed, bone will remodel so that the stress or strain is retained within specific levels. Aseptic loosening of the prosthesis in the case of total hip replacement, due to bone resorption in the proximal femur is believed to be caused by the state of stress and strain in the femoral cortex after the metallic femoral hip replacement is implanted. Elastic characteristics of the implant play a significant role in allowing the femur to attain a physiologically acceptable stress state. In order to overcome the problem of modulus-mismatch between existing implant materials and bone and promote the formation of a secure bond between the implant and host tissue, the concept of analogue biomaterials was introduced in the 1980s (Wang et al. 2003). Since then, a variety of bioactive composite materials have been produced and investigated.

In the development of new engineering materials, apart from other required properties, strong and stiff materials coupled with reasonable ductility are always targeted. In developing new biomaterials for tissue replacement, the structure and

properties of the tissue which is to be replaced must be taken into consideration, because, if properties of the new material are significantly different from those of the host tissue, the material under development will cause dynamic changes in the host tissue after implantation, as has been discussed in terms of Wolff's Law, and thus will not achieve the goals considered in the original conceptual design.

Bone serves as the template for making new materials for hard tissue replacement. Bone is a natural composite material, having a complex structure in which several levels of organization, from macro to micro-scale, can be identified. Two levels of composite structures are considered when developing bone substitutes: first, the bone apatite reinforced collagen forming individual lamella at the nm to micron scale and, second, osteon reinforced interstitial bone at the micron to mm scale (Wang et al. 2003). It is the apatite-collagen composite at the microscopic level that provides the basis for producing bioactive ceramic-polymer composites as analogue biomaterials for bone replacement.

2.6. Bone

Bone is a ceramic-organic composite that has a complex structure. The main constituents of bone are collagen (20 wt. %), calcium phosphate (69 wt. %), and water (9 wt. %). Additionally, small quantities of other organic materials, such as proteins, olysaccharides, and lipids are also present. Collagen, which can be considered as the matrix, is in the form of small microfibers which have diameters in the100-2000 nm range. It is difficult to observe distinct collagen fibers because of its net-like mass appearance. Calcium phosphate provides stiffness to the bone and is in the form of crystallized carbonated hydroxyapatite and/or amorphous calcium phosphate. In between collagen molecules there are small interstitial empty compartments, regularly spaced, where apatite nanocrystals are deposited, in a controlled biomineralization process involving more than 200 different acid proteins. These proteins act as inhibitors, nucleators or templates for the epitaxial growth of nanocrystals, anchored to the collagen. The crystallization of the complex and hardly soluble apatite structures evolves favourably through the kinetically controlled formation of metastable intermediate products. The HA crystals are oriented parallel to the collagen fibers in the form of plates or needles that are about 40–60 nm long, 20 nm wide, and 1.5–5 nm

thick. The carbonate hydroxyapatite of bones ranges between 4% and 8% in carbonate content, which increases with age while the hydrogen phosphate ion decreases (Suchanek et al. 1997).

Bones are characterized by their composition, crystalline structure, morphology, particle size and orientation. Compact and cancellous are two main forms mature bone exists. In compact bone the mineral-containing fibers are arranged into lamellar sheets a few millimeters thick. 4–20 lamellae arranged in concentric rings around the Haversian canal form an osteon. Blood vessels are located in the center of each osteon inside Haversian canals. The metabolic substances can be transported by the intercommunicating systems of canaliculi, lacunae, and Volkman's canals, which are connected with the marrow cavity. The various interconnecting systems are filled with body fluids and their volume can be as high as 19%. Cancellous or trabecular bone is a spongy cellular material consisting of a connected network of rods or plates as shown in Figure 1. Low density, open cell, rod-like structures develop in regions of low stress while high density, closed cell, plate-like structures occur in regions of higher stress (Suchanek et al. 1997).

Bones can be considered as ''living biominerals'' since there are cells inside them under permanent activity. The bone formation process starts by the action of osteoblasts, special cells that synthesize and release the collagen matrix in the form of a jelly substance, the osteoid, which is subsequently mineralized by controlled deposition of calcium phosphate. The osteoblasts remain trapped inside the mineral phase, evolving towards osteocites which continuously maintain the bone formation activity. Meanwhile, another type of cells called the osteoclasts catabolyse the bone destroying it. This dynamic process of bone formation and destruction accounts for its growth during the development stages of the body, preserving its shape and consistency, and enabling its regeneration in case of fracture (Vallet –Regi et al. 2004). It also constitutes a storage and hauling mechanism for two essential elements, phosphorus and calcium, which are mainly stored in the bones. The bones can exhibit different types of integration between organic and inorganic materials, leading to significant variations in their mechanical properties. The ratio of both components reflects the compromise between toughness (high inorganic content) and resiliency or fracture strength (low inorganic content). Mechanical properties of a compact bone is given in Table 7.

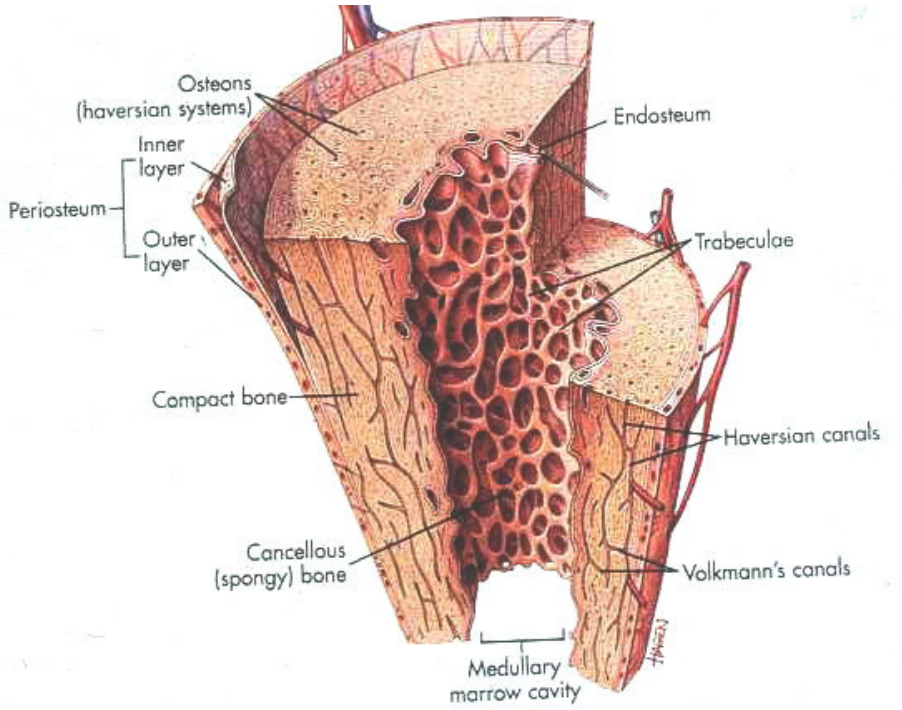

Figure 1. The structure of bone

(Source: http://pathologyoutlines.com/bone.html)

Table 7. Mechanical properties of a compact human bone

	Test direction related to bone axis	
	Parallel	Normal
Tensile strength (MPa)	124-174	49
Compressive strength (MPa)	170-193	133
Bending strength (MPa)	160	
Shear strength (MPa)	54	
Young's modulus (GP)a)	17.0-18.9	11.5
Work of fracture (J/m^2)	6000	
K_{Ic} ($MPa*m^{1/2}$)	2-12	
Ultimate tensile strain	0.014-0.031	0.007
Ultimate compressive strain	0.0185-0.026	0.028
Yield tensile strain	0.007	0.004
Yield compressive strain	0.010	0.011

2.7. Properties of Bone Implants

A bone-graft substitute should be osteoconductive, osteoinductive, biocompatible, bio-resorbable, structurally similar to bone, and undergo remodelling. Ideally, a bone implant such as a hip implant should be such that it exhibits an identical response to loading as real bone and is also biocompatible with existing tissue. A ceramic with higher porosity and lower density construct provides greater surface area for vascularisation, and bony ingrowth. The optimal conditions for osteoconductivity are a narrow distribution of interconnective pores with size in the range 150-300 microns (Chang et al. 2000). The arrangement of the pores and size of the interconnectivity are influential on mechanical properties as well as the osteoconductivity. The osteoconductive scaffold provides an appropriate environment for bone cells and bone proteins. The newly placed osteoconductive ceramic that lacks mechanical bone characteristics, gradually acquires mechanical strength similar to cancellous bone due to growth of bone after incorporation.

The design of bioceramic bone substitute implants is still not practical since their inherent rigidity and breakability are the main drawbacks in load-bearing applications. The applications of bioceramics are currently focused on the production of non-load-bearing implants, such as pieces for middle ear surgery, filling of bone defects in oral or orthopaedic surgery, and coating of dental implants and metallic prosthesis. This inadequacy of bioceramics is targeted to be overcome by synthesis of nanostructured ceramics similar to the complex hierarchical structures of hard tissues having improved mechanical strength. A Synthetic bone substitute should have similar strength to that of the cortical/cancellous bone being replaced (>200MPa). It should also have a similar modulus of elasticity to that of bone (≥20GPa) in an attempt to prevent both stress shielding and fatigue fracture under cyclic loading by maintaining adequate toughness (Giannoudis et al. 2005).

CHAPTER 3

BIOCOMPOSITE PROCESSING

Major drawbacks of all biocompatible ceramics restrict their use in biomedical applications to some degree. Low strength and fracture toughness of hydroxyapatite limits its bulk use in many implants. As ZrO_2 ceramic is a bioinert material, it does not directly bond with natural bone in hip-joint replacement. Alumina's high elastic modulus causes stress shielding that results in loosening of implants in patients with osteoporosis.

The preparation of a microscale composite material is a promising idea for improving the mechanical properties of hydroxyapatite. HA may be reinforced with other ceramics or metals in the form of powders, platelets, or fibers. This approach has been the subject of extensive study since the successful development of ceramic-matrix composite materials. In order to synthesize an effective ceramic-matrix composite material, three conditions should be satisfied. The strength and the stiffness of the reinforcement must exceed those of the matrix. Along with this requirement the strength of the interfacial layer between the matrix and the reinforcement should be appropriate with limited reaction between the matrix and the reinforcement producing a bond strength neither too weak nor too strong. Also, the difference between the coefficients of thermal expansion of the phases should be low enough to prevent formation of microcracks during cooling. The absence of these conditions provides microstructural defects resulting in deterioration of the mechanical properties of the composite (Kim et al. 1999). The biocompatibility of the reinforcement phase should also be considered when the ceramic matrix composite is designed to be involved in biomaterials applications.

Most metals react with the HA to form metal oxides and tricalcium phosphate (TCP, $Ca_3(PO_4)_2$) or tetracalcium phosphate (TeCP, $Ca_4(PO_4)_2O$), leading to a serious reduction in the biocompatibility of HA. Partially stabilized zirconia has been commonly used as reinforcement for many ceramics because of its high strength and fracture toughness. Bioinertness is another merit of the ZrO_2. However, extensive reaction between the HA and the ZrO_2 to form TCP and fully stabilized ZrO_2 is a big disadvantage of this approach. Alumina, which is also classified as a bioinert material,

has been widely investigated as a reinforcing agent for HA. When large alumina platelets were added, the fracture toughness of the HA increased without excessive reaction between the HA and the Al_2O_3. However, the improvement in strength was minimal because of the formation of microcracks around the platelets due to the large difference in coefficient of thermal expansion between Al_2O_3 and HA. On the other hand, when fine Al_2O_3 powder was used, the formation of the microcracks was circumvented; however, the improvement in mechanical properties was limited due to relatively low mechanical properties of the Al_2O_3 itself (Kim et al. 2004). Therefore, it is desirable to combine the advantages of both materials as reinforcements for the HA: the excellent mechanical properties of ZrO_2 and the chemical inertness of Al_2O_3 with respect to the HA.

In a study on the formation of alumina and alumina–zirconia minispheres by sol–gel processing, a composite with maximum density 91% theoretical was obtained with the optimum zirconia amount of 10wt% and the microstructure of this composite is shown in Figure 2 (Katti et al. 2004). Homogeneous crystal grain structure with interconnectivity is obtained with fine grain sizes of 30 nm by another sol-gel synthesis study of HA-zirconia composites and their microstructures are given in Figure 3 (Balamurugan et al. 2005).

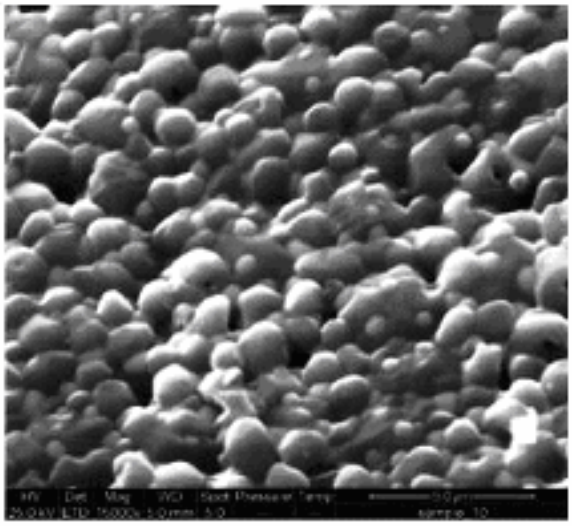

Figure 2. SEM image of alumina-zirconia composite
(Source: Katti et al. 2004)

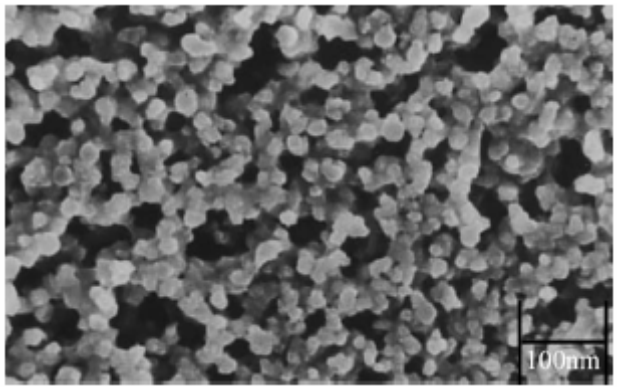

Figure 3. SEM image of zirconia-HA composite
(Source: Balamurugan et al. 2005)

4.1. Transformation Toughening

Transformation toughening is one of the mechanisms of increasing crack growth resistance in materials. The increase in toughness is provided by martensitic transformation of the microstructure to a metastable phase that returns to stable state with a pressure or temperature effect from the surrounding. In a normal ceramic crack travels all the way through the ceramic with little inhibition, resulting in immediate brittle fracture. While in transformation toughened material the crack can not propogate as its motion is inhibited by strain field around transformed reinforcement. Two classes of materials exhibit transformation toughening: zirconia containing ceramics and transformation induced plasticity steels. Transformation toughened zirconia has fracture toughness 3–6 times higher than normal zirconia and most other ceramics. It is tougher than cast iron and comparable in toughness to WC-Co cermet (Stevens et al. 1986).

Zirconia has the monoclinic crystal structure between room temperature and about 950 ^{o}C . Above 950 ^{o}C zirconia converts to the tetragonal crystal structure shown in Figure 4. This transformation is accompanied by greater than three percent shrinkage during heating and equivalent expansion during cooling. At a much higher temperature, the zirconia transforms from tetragonal to cubic structure. With proper chemical additions and heat treatments, a microstructure can be achieved during cooling that consists of precipitates of tetragonal zirconia in cubic grains of zirconia (PSZ). Normally, the tetragonal material transforms to the monoclinic form during cooling accompanied by an expansion. The high strength of the surrounding cubic zirconia

prevents this expansion, so the tetragonal form is retained during cooling to room temperature. As a result, each tetragonal zirconia precipitate is under stress with strain energy that has to be released. Each tetragonal precipitate releases energy and expands to stable size in monoclinic form if a crack tries to form under stress. Transformation toughening is provided by the pressure of this expansion adjacent to the crack against the crack as shown in Figure 5.

The martensitic t→m transformation is induced by cooling or by external loading under isothermal conditions. Thermally induced transformation controls the amount of tetragonal phase that can be retained after thermal cycling and the stress induced martensitic transformation enhances the toughness of zirconia ceramics.

The tetragonal to monoclinic transformation is a isothermal martensitic transformation, associated with a large temperature hysteresis in the order of several hundred K, a volume change or dilation component of transformation strain (4– 5%) and a large shear strain (14–15%). Large shear strain leads to disintegration of sintered undoped zirconia parts. For this reason dopants like yittria, ceria, magnesia are added to stabilize the high temperature tetragonal and/or cubic phase in the sintered microstructure (Jin et al. 2006).

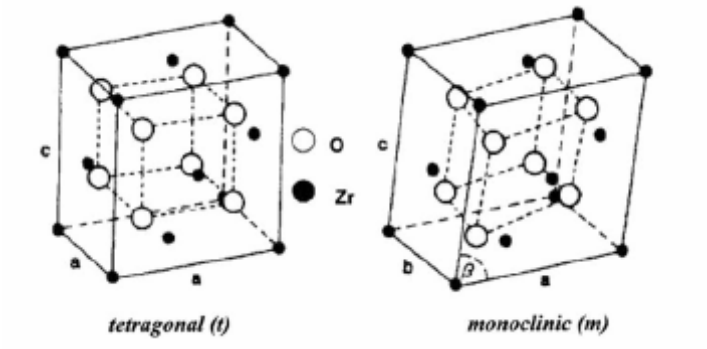

Figure 4. Two low temperature polymorphs of zirconia
(Source: Jin et al. 2006)

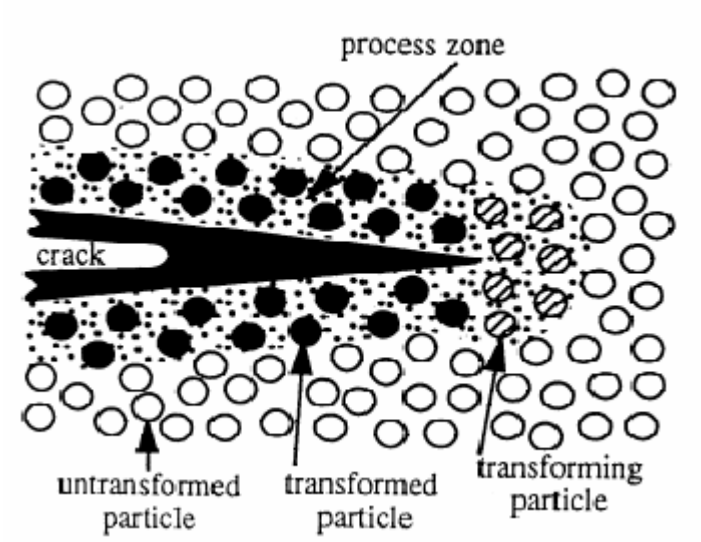

Figure 5. Schematic of resistance to crack propagation in transformation toughened material (Source: Piconi et al. 1999)

Apart from crack deflection that occurs in two phase materials, two different mechanisms may help zirconia develop significantly improved properties via t→m transformation. Microcracking which can be induced by the incorporation of ZrO_2 particles in a ceramic matrix is crack formation around ZrO_2 particles by volume expansion (4-5%) on cooling through the transformation temperature $T_{t\rightarrow m}$. Tangential stresses generated around the transformed particle induce microcracks in the matrix. The toughness of the ceramic is increased by absorption and dissipation of the energy of a crack by the ability of the microcracks to extend in the stress field of a propagating crack. Particle size of the ZrO_2 phase is important as it has to be large enough to transform and small enough to cause limited microcrack development. The interactions of microcracks generated by each zirconia particle needs to be avoided for maximum strength by setting the volume fraction of zirconia phase to an optimum value (Stevens et al. 1986).

The other mechanism of toughening is stress induced transformation of metastable tetragonal particles, which are retained in the metastable form in constraining pressure of matrix through cooling to room temperature, to the monoclinic form. Large tensile stresses are generated ahead of an extending crack tip that release the matrix constraint on the tetragonal zirconia particles and result in a net tensile stress on the particle, transforming it to monoclinic form. A resultant compressive strain with >3% volume expansion and 1-7% shear strain hinders the movement of the crack in the

vicinity, increasing the toughness and strength of the ceramic. A critical particle size exists as a function of stabilizer content below which the particles do not transform and above which spontaneous transformation occurs. With increasing cubic stabilizing oxide content the chemical free energy associated with the phase transformation decreases and larger particles can be induced to remain in metastable tetragonal form.

4.2. ZrO_2 Reinforced Composites

Zirconia containing ceramics are materials of imparting toughness while maintaining strength and chemical inertness. These properties can be achieved by transformation toughening in ceramic materials by addition of particles of partially stabilized zirconia through structure transformation from tetragonal (t) to monoclinic (m). Toughening occurs if the particles are small, if the host ceramic is strong enough to prevent the particles from transforming during cooling, and if there is no chemical interaction between the materials. Alumina is the most important ceramic that is a suitable host for zirconia toughening. An addition of 15–25% zirconia to alumina results in toughness and strength nearly equivalent to that of pure transformation toughened zirconia (Jin et al. 2006).

The most common zirconia toughened ceramic system is Al_2O_3-ZrO_2 where particles of pure zirconia or partially stabilised zirconia are added to Al_2O_3 powder, mixed, sintered or hot pressed. Much research done on this system reveals that there is a considerable increase in strength and toughness as a result of particle sizes of pure zirconia of 1-2 microns and of PSZ of 2-5 microns and also with optimum volume fraction of 15% ZrO_2 in Al_2O_3 (Stevens et al. 1986).

Zirconia is used as reinforcement phase in other matrix materials. Spinel, mullite, silicon carbide have shown improvements in toughness and strength by zirconia addition. The zirconia reinforced ceramics are used in cutting tool tips, wear parts of many components, internal combustion engine components, and seals where a combination of wear resistance, flexural strength and corrosion resistance is required.

Zirconia reinforced composites can be prepared by routes other than mechanical mixing of the precursor oxide, sol-gel processing, solid-liquid mixing and precipitation methods followed by drying, calcining, forming and sintering. Optimization of the sintering cycle is important since the matrix is required to reach a high density in order to give the necessary mechanical constraint to the zirconia particles.

Design of a multiphase system can be made in microscale so as to use properties of zirconia to advantage, more efficiently than simple composite systems mentioned above. A duplex microstructure using a polycrystalline agglomerate of metastable zirconia in a matrix of fine grained alumina offers a structure that takes advantage of both phases optimally. Toughening mechanisms of crack deflection, microcracking, and crack pinning are present in this type of material where small islands of zirconia reinforcement act as crack inhibitors. Such microstructure is seen to develop fracture strengths greater than 700 MPa and $K_{IC} > 12$ MPa $m^{1/2}$ (Stevens et al. 1986). Zirconia has a lower elastic modulus than the matrix which results in movement of the cracks toward the zirconia particles and the energy of the crack can be absorbed by the effective concentration of zirconia particles in the agglomerates. This microstructure is more efficient at stopping cracks than if the zirconia had been uniformly dispersed throughout the matrix. The duplex structure can further be enhanced by dispersing transformed zirconia particles in the matrix, as a result placing the matrix in compression and causing a further driving force for propagating critical cracks to move to the zirconia agglomerates.

Hydroxyapatite-zirconia composites have been synthesized as an effort to produce bone graft substitute materials with improved mechanical properties. Similar reinforcement effect is obtained from these composites to Al_2O_3-ZrO_2 composites. During heating of HA–ZrO_2 materials desirable effects, such as the T↔M transition of the monoclinic ZrO_2 into the tetragonal polymorphic form and its stabilisation by CaO originating from hydroxyapatite, as well as the formation of a solid solution of CaO in ZrO_2 appear. It has been reported, however, that the addition of ZrO_2 to the HA matrix decreases the temperature of hydroxyapatite decomposition (Rapacz-Kmita et al. 2006). This leads to uncontrolled and not always desirable changes of physicochemical and biological properties of the materials. It is important to avoid decomposition of HA by zirconia through careful heat treatment or reducing physical contact between the phases because potential products of decomposition like $CaZrO_3$ can significantly influence the behaviour of a material in body. A comparison of properties of HA–ZrO_2 composites and other reinforcement phases in hydroxyapatite is given in Table 8 (Rapacz-Kmita et al. 2006).

Table 8. Reinforced HA composites comparison table

Reinforcement	Relative density (%)	Flexural strength (MPa)	K_{Ic} ($MPa*m^{1/2}$)	Phase composition (calcium phosphates)	Processing
5-30 vol. % Al_2O_3 particles	96-99.7	90-250	1.4-2.5	HA, β-TCP	HP (1000-1250 °C)
10 vol. % fibers (ZrO_2, Al_2O_3, C)	68-82	---	---	HA, β-TCP	Sintering (1000-1150 °C)
5 wt% SiC nanoparticles	---	110	2.1	HA	---
10-50 vol.% (3Y)ZrO_2	93-99.5	160-310	1.0-3.0	HA, β-TCP, α-TCP	HP (1050-1400 °C)

4.3 Coating of Particles by Heterogeneous Precipitation

Heterogeneous precipitation is a processing method for ceramic-ceramic composite powders which involves several steps as follows. Preparation starts by forming a suspension through mixing an inorganic powder having a cation exchange property with a solution containing one or more metal ions to conduct ion exchange with the metal ions on the surface of the inorganic powder. This is followed by adding a precipitant-forming reagent to the suspension that releases an anion in a solution when heated or pressurized and heating or pressurizing the suspension to release the anion which reacts with the metal ions to thereby precipitate metal hydroxides, metal basic salts or metallic salts on the surface of the inorganic powder. Resultant precipitates are further calcined to convert them into metal oxides.

Heterogeneous precipitation is the most commonly used method for powder coating for core-shell structure. By this method ceramic-ceramic composite powders in which metal oxides are uniformly supported on the surface of an inorganic powder can be obtained by precipitating metal hydroxides, metal basic salts, or metallic salts uniformly on the surface of the ceramic core and then calcining the resultant composite powders. Metal-ceramic composite powders in which the inorganic powder is uniformly coated with the metal, can be obtained by reducing the metal oxides to metal.

For the formation of precipitates by using the precipitant-forming material, the suspension added with the material is either heated at a temperature in the range of from about room temperature to about the boiling point; pressurized at the range of from

about 1 to about 150 atms, or simultaneously heated and pressurized in the above ranges so that the precipitant-forming material in the suspension is uniformly and gradually decomposed to release the anion. Metal hydroxides, metal basic salts, or metallic salts are then gradually precipitated on the surface of the inorganic ion-exchanger core. Thus, the nuclei grow on the fixed metal ions which are introduced on the surface of the ion-exchanger by ion exchange, followed by the precipitation at the nucleation sites (Ohtsuka et al. 1991).

The precipitant forming agent; which may be urea, acetamide, formamide, various esters (dimethyl oxalate, diethyl oxalate, trimethylphosphoric acid, triethylphosphoric acid, dimethylsulfuric acid, diethylsulfuric acid), amidosulfuric acid, sulfur containing compounds (thioacetamide, thiourea, ammonium thiocarbanate) and trichloroacetate; releases various anions by hydrolysis. In the case of urea in an aqueous solution, upon heating urea is hydrolyzed to cause the reaction shown in the formula:

$$(NH_2)_2CO+3H_2O \rightarrow 2NH_4^+ + CO_2 + 2OH^- \quad (2)$$

The above reaction produces anions, such as, OH^- and CO_3^{2-}. If metal ions are present they react with the above anions to form precipitates comprising metal hydroxides, metal carbonates, or metal basic salts. Any substance that can decompose at certain temperature and pressure in a solution may be used as a precipitant-forming material in homogeneous precipitation method. Uniform precipitation of the metal hydroxides, metal basic salts, or metallic salts on the surface of intentionally added inorganic powders with the cation-exchange properties can thus make the synthesis of composite powders with unique properties.

Core-shell coating with urea decomposition was conducted succesfully in an attempt to coat $BaTiO_3$ with MgO (Han et al. 2006). Homogeneous and narrow MgO shell regions were obtained by mixing a suspension of $BaTiO_3$ and 3 mol% MgO at 90°C for 2 hours and then calcining at 700°C. Uniform precipitation of magnesium hydroxide on the $BaTiO_3$ surface is facilitated by the hydrolysis of urea and hetero-coagulation of the core and shell particles.

Smooth TiO_2 coating with a thickness of 20 nm is obtained in the study of heterogeneous precipitation of TiO_2 on α-Al_2O_3 with an average size of 0.5 microns. Titanium tetrabutoxide is hydrolyzed in an alumina suspension containing excess urea

at continious mixing for 48 hours at 80°C. Subsequent calcining at 500°C produced homogeneous TiO_2 coating on α-Al_2O_3 (Villegas et al. 2006).

In a study of calcium deficient hydroxyapatite synthesis in the presence of decomposing urea, hydroxyapatite fibers were precipitated using sub-stoichiometric calcium nitrate, ammonium phosphate and urea/calcium nitrate ratio of 5. Apatite fibers as long as 100 microns were obtained by heating the mixture at 90°C for 24 hours. Thicknessesof the fibers were found to decrease with increasing Ca/P (Aizawa et al. 2006).

Effect of urea amount on the properties of precipitated TiO_2 particles were observed in a synthesis that involved preparing a suspension with urea content between 0 and 1200 times molar concentration of the precipitant. It is found that urea content influenced the crystal phase, deposition rate, and the specific surface area of the precipitated particles. Rutile and anatase phases were formed with urea/$TiOSO_4$ ratios between 0-75 and 150-500 respectively. A two-fold increase in urea amount doubled the deposition rate and the specific surface area increased from 150 to 350m^2/g with changing urea amount from 0 to 300 times the precipitant (Imai et al. 2003).

When coating uniformity and thickness are concerned, parameters of importance in heterogeneous precipitation are the temperature and stirring conditions of the aqueous medium, duration of stirring and ratio of urea to precipitant.

4.5. Core-Shell Approach

A ceramic composite on the nanoscale has advantages of homogeneity, higher mechanical properties due to finer microstructure in the bulk form. The versatility of the nanoscale composite powder to be shaped into complex shapes with desired porosity degree is another advantage. Nanocoating of the components of the zirconia-alumina-hydroxyapatite composite on each other promises potential for a bioceramic material with exceptional properties. The proposed model for this synthesis is three layer particulates with core-shell structure. Y-TZP core at the center, alumina layer coated on the core, and a thicker hydroxyapatite layer over the inner coating of alumina is aimed to form. As mentioned in previous chapters the reinforcement effect of zirconia polycrystals is at peak with a zirconia volume fraction near 10%. Taking the nanocomposite particle as a model for the whole bulk material, the fraction of the

zirconia in the material is set to 10 volume % as the small core in the material. The intermediate alumina layer consisting of 20 volume % of the material is projected to block physical contact of zirconia and hydroxyapatite phases that react to form impurity phases and to transmit the propagating cracks from hydroxyapatite to zirconia as illustrated in Figure 6. Hydroxyapatite outer layer on the nanocomposite particles formed 70% of the material by volume and provides the matrix phase in the sintered bulk form. Sintered bulk material is designed to be a continous hydroxyapatite matrix dispersed with alumina coated zirconia reinforcements that take advantage of useful properties of the two strong reinforcements. As the nano-sized particles are closely packed, the sintering mechanism is dependent only on the sintering of hydroxyapatite phase and the sintering temperature is set in accordance to that and to the decomposition temperature of hydroxyapatite.

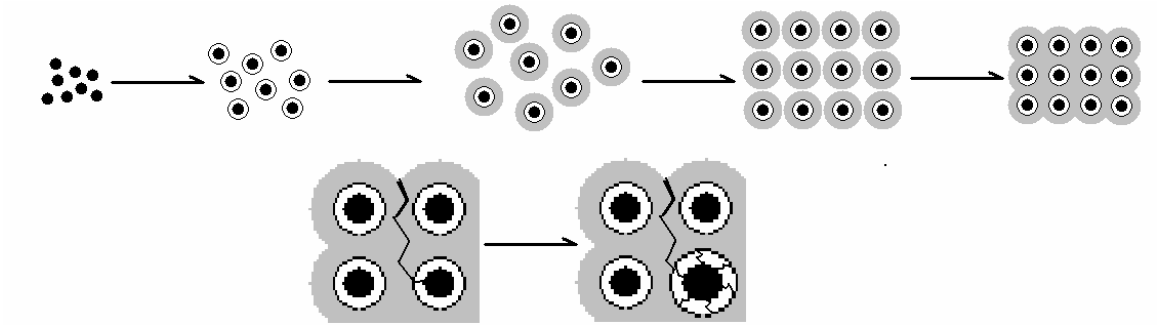

Figure 6. Schematic of the composite synthesis

The core-shell structure powders are aimed to be synthesized by urea heterogeneous precipitation method. A two step process in which alumina coated zirconia particles are first prepared and HA coating layer is applied on the core particles is suitable . Subsequent treatments including calcination, consolidation and sintering are required to obtain a dense bulk ceramic composite.

4.5 Preparation of Porous Materials

Biomaterials having a porous structure are ideal for bone graft substitution because of the ability of the porous structure to mechanically fix the implant and provide host sites for osteoblasts and osteoclasts in the interconnected pore channels.

The ideal artificial bone demands good biocompatibility without the possibility of inflammation or foreign body/toxic reactions. Strong bonding with the host bone, active bone ingrowth into the graft, and bioabsorbability are also required. Sufficient strength to resist the mechanical load in the implanted bone is also needed. None of the biomaterials that have been developed unill now meet all of these criteria. HA has good biocompatibility and osteoconductivity, however its fragility is a drawback like most ceramic materials. Therefore, it can be used alone in areas that do not require good mechanical strength. It can also be used with supplementary metal fixation in areas which bear large amounts of the mechanical load. The structure of the dense sintered body is stronger and more able to bond rapidly with host bone, but its use is limited due to its high level of brittleness and low osteoconductivity and absorbability. Porous HA is considered a good substitute, because it shows good osteoconduction and is replaced by the host bone although it is mechanically weak. Patterns of osteoconduction for porous HAs vary with pore configuration. In HA, the 50 micron sized pore is enough, and the 300 micron sized pore is optimum for osteoconduction (Chang et al. 2000). Porous HA can be a useful graft material due to its osteoconductivity and the ease with which its pore geometry can be controlled.

The simplest way to generate porous scaffolds from ceramics such as HA is to sinter particles, preferably spheres of equal size. With the increase in temperature pore diameter decreases and mechanical properties increase as the packing of the spheres increases. Hot isostatic pressing can also be used to further decrease the pore diameter. During sintering porosity can be increased by adding fillers such as sucrose, gelatine, and PMMA microbeads to the powder and the wetting solution. One of the most reliable formulations is the use of an HA powder slurry with gelatine solution. Surface tension forces cause the formation of soft and spherical porous particles of HA and gelatine. It is possible to produce porous bulk material with an interconnected pore structure with an average pore size of 100 microns after sintering (Taş et al. 2004).

It is possible to produce interconnected pores with diameters up to 300 microns by using the polymer foam replication method. Open celled polyurethane foams can be immersed in ceramic slurries under vacuum to allow the slurry to penetrate into the pores of the foam. Burn out of foam at 250 °C produces the ceramic replica of the foam. Using a similar method hydroxyapatite coated zirconia scaffolds with interconnected pore diameters up to 500 microns have been produced (Jones et al. 2003). Zirconia's enhanced strength allows a high percentage of porosity in the composite.

Highly porous ceramics can be produced through foaming particulate suspensions or colloidal sols to obtain pores in the range of 20 microns to 1-2 mm. By injection of gases through the fluid medium, mechanical agitation, and decomposition of some organic-inorganic components formation of pores in the bulk material is achieved. As a result direct foaming of the ceramic is maintained.

Gel casting method is the most suitable method for producing optimum size porosity since foam volume and porosity can be controlled by the surfactant concentration in the slurry (Zhang et al. 2003). Suspensions of HA particles, water, dispersing agents and organic monomers are foamed by agitation with addition of a surfactant under inert atmosphere. In situ polymerization of the monomers is initiated and cross-linking occurs, forming a polymeric gel network which produces strong green bodies. Porous samples are sintered to provide mechanical strength and to burnout the organic additives, producing pores in the range of 100-200 microns.

One other method for producing porous ceramics is freeze drying. Freeze drying process can be used to introduce aligned pores in the final ceramic structure but the generated pore diameters do not exceed 10 microns.

CHAPTER 4

EXPERIMENTAL PROCEDURE

4.1. Wet Mixing of Composite Components

Commercial 3mol% yttria added tetragonal zirconia (TZ-3Y, Tosoh), alumina (AKP-50, Sumitomo), and hydroxyapatite (Aldrich) were used in synthesis of mechanically mixed composite samples. A number of sample sets of different compositions of components were prepared from 30 v% HA to 70 v% HA and 10-30 v% TZ-3Y of the remaining two phase mixture (Table 9). For all samples proportional weights of TZ-3Y, alumina, and hydroxyapatite were mixed and ultrasonically treated for 1 hour in distilled water at 1:20 volume ratio for homogeneous mixing. Ultrasonically treated well mixed powder suspensions were dried at 100 °C in an oven for 6 hours and crushed with a mortar and pestle. Pellets were prepared from 0.4 grams of each powder sample at a pressure of 160 MPa. Sizes of the green pellets were approximately 10 mm in diameter and 2 mm in height. The pelletized samples were sintered at different temperatures of 1100 °C, 1200 °C, 1250 °C, and 1300 °C. The sinterability, phase transformations, and density of the samples at sintering temperatures of 1100 to 1300 °C were further investigated. Morphological structure was investigated by SEM, porosity of the pellets by archimedes' method, phase purity by XRD.

Table 9. List of samples prepared with varying compositions

Sample	Hydroxyapatite content	Alumina content	Zirconia content
1	30 vol %	63 vol %	7 vol %
2	30 vol %	56 vol %	14 vol %
3	30 vol %	49 vol %	21 vol %
4	50 vol %	45 vol %	5 vol %
5	50 vol %	40 vol %	10 vol %
6	50 vol %	35 vol %	15 vol %
7	70 vol %	27 vol %	3 vol %
8	70 vol %	24 vol %	6 vol %
9	70 vol %	21 vol %	9 vol %

4.2 Urea Heterogeneous Precipitation Method

Heterogeneous precipitation method was applied for the synthesis of alumina coated zirconia cores and HA coated alumina-zirconia nanocomposites using urea as the precipitation agent. The chemicals used in the experiment are given in the following table

Table 10. Chemicals used in this work

Powders/Chemicals	Chemical Formula	Formula Weight	Purity/Source	Form
TZ-3Y	ZrO_2-3%Y_2O_3	126.3 gr	99% TOSOH	Powder <180nm
Aluminum Sulfate Hydrate	$Al_2(SO_4).xH_2O$	342.2 gr	98% ALDRICH	Pellet
Calcium Nitrate Tetrahydrate	$Ca(NO_3)_2.4H_2O$	236.1 gr	99% SIGMA	Powder
Ammonium dihydrogen Phosphate	$(NH_4)H_2PO_4$	132.2 gr	99% MERCK	Powder
Urea	$CO(NH_2)_2$	60.06 gr	99% MERCK	Powder

4.2.1 Alumina-Zirconia Composite Powder Synthesis

Preliminary experiments were conducted with varying aluminum sulfate and urea concentrations for the determination of the optimum urea/aluminum sulfate ratio for the particular 10:20 volume ratio of alumina and zirconia phases. The purpose for running these preliminary experiments was to correlate the relative compositions of the starting precursors to the results obtained from characterization data and to find the most suitable precursor composition for complete coating.

For the synthesis of alumina-zirconia nanocomposite samples Tosoh TZ-3Y powder with average particle size of 180 nm, aluminum sulfate hydrate, and urea were used. Variable amounts of aluminum sulfate were added to a specified amount of TZ-3Y and urea was dissolved in the aqueous solution with molar ratio changing between 3-12 per mole of aluminum sulfate as given in Table 11. Aluminum sulfate and TZ-3Y

were added simultaneously to faciliate contact and attachment of aluminum precursor on the surface of TZ-3Y cores. 500ml of the mixture was stirred on hot plate for varying durations from 2 to 6 hours. Temperature was kept above 85 °C during stirring for decomposition of urea. The extent of the coating is determined by particle size measurements from both SEM and Zetasizer. Phase purity before and after calcination was investigated. Some samples were calcined after synthesis to observe the effect of calcination on coating with HA.

Powders obtained after synthesis were cleaned off any impurities and unreacted sulfate and urea species by centrifuging at 5000rpm for 15 minutes and throughly washing with distilled water. Wet powders were dried in oven at 80 °C for 12 hours for subsequent characterizaton. For zetasizer and SEM analysis sample powders were ultrasonically agitated in order to break down of agglomerates. For densification and sinterability studies powders were uniaxially pressed in dies of 10 mm diameter at a pressure of 160 MPa.

Table 11. Composition of the alumina coated zirconia samples

Urea Alumina Coatings on TZ-3Y						
	Al. Sulf.	TZ-3Y	Urea	Characterization		
AZ1	3.422gr	0.6315gr	1.802gr	Zetasizer	SEM	EDX
AZ2	3.422gr	0.3157gr	3.6036gr	Zetasizer	SEM	EDX
AZ3	3.422gr	0.3157gr	7.2gr	Zetasizer		
AZ4	3.422gr	0.3157gr	3.6036gr	Zetasizer	SEM	EDX
AZ5	3.422gr	0.3157gr	7.2072gr	Zetasizer		
AZ6	6.844gr	0.3157gr	3.6036gr	Zetasizer		
AZ7	1.711gr	0.3157gr	1.802gr	Zetasizer	SEM	EDX
AZ8	17.11gr	1.5785gr	18.018gr	Zetasizer		
AZ9	17.11gr	1.5785gr	18.018gr	Zetasizer		
AZ10	17.11gr	1.5785gr	18.018gr	Zetasizer		
AZ11	17.11gr	1.5785gr	18.018gr	Zetasizer	SEM	
AZ15	6.77 gr	1.5785gr	11.87 gr	Zetasizer	SEM	EDX
AZ20	17.11gr	1.5785gr	18.018gr	Zetasizer		
AZ21	3.422gr	0.3157gr	3.6036gr		SEM	EDX
AZ22	6.87gr	1.5785gr	11.87gr		SEM	EDX
AZ24	17.11gr	1.5785gr	29.56gr	Zetasizer	SEM	EDX
AZ25	6.87gr	1.5785gr	7.2gr	Zetasizer	SEM	EDX

4.2.2 Hydroxyapatite Coating on Alumina-Zirconia Cores

HA coating on alumina-zirconia nanocomposites was applied using urea heterogeneous precipitation with precursors calcium nitrate tetrahydrate, ammonium phosphate, urea and alumina-zirconia nanocomposite cores. The samples were synthesised with a fixed relative precursor amount between cores, calcium nitrate and ammonium phosphate according to the volume percent ratio of 10:20:70 for zirconia, alumina and HA as given in Table 12. The Ca/P precursor ratio was kept at 1.67 for stoichiometric HA formation. The pre-coated zirconia-alumina composites were used as cores and added to 500ml of distilled water at the beginning of the process. Attachment of calcium ions on aluminum hydroxides on the surface of the cores was maintained by dissolving calcium nitrate at the same time the cores were added and waiting for complete surface attachment between the two precursors. Heating the mixture above 85 °C and adding the precipitating agent urea with ammonium phosphate results in formation of calcium phosphate complexes on the surface of the cores with calcium phosphate precipitation with the decomposition action of urea. Aqueous medium was kept at pH 10 by addition NH_4OH during precipitation of HA. Evaluation of the coatings was done by zetasizer and SEM analysis for comparison of core and coated particle sizes, EDX and XRD analysis for composition investigation and phase purity, TGA for thermal stability.

Table 12. Composition of hydroxyapatite coated core samples

Urea HA coatings on Alumina-Zirconia cores							
	Core	Urea	Ca Nit.	Amm. Phos.	Characterization		
AZH5	0.5 gr AZ5	4.3 gr	1.705gr	0.573 gr	Zetasizer	SEM	EDX
AZH7	0.1 gr AZ7	1.13 gr	0.446gr	0.115 gr	Zetasizer		
AZH10	0.5gr AZ9	4.3 gr	1.705gr	0.573 gr	Zetasizer	SEM	
AZH18	2.1 gr AZ15	20.6 gr	8.1 gr	2.72 gr	Zetasizer	SEM	EDX
AZH19	1gr AZ4	8.6 gr	3.41gr	1.146gr	Zetasizer	SEM	EDX
AZH20	0.97gr AZ7	8.4 gr	3.39gr	1.12gr	Zetasizer	SEM	EDX
AZH22	0.5gr AZ21	4.3gr	1.705gr	0.57gr		SEM	EDX
AZH23	1.04gr AZ22	8.6gr	3.41gr	1.15gr		SEM	EDX
AZH25	1.2gr AZ24	8.6gr	4.1gr	1.4gr	Zetasizer	SEM	EDX
AZH26	3.33gr AZ25	28.9gr	11.35gr	3.83gr	Zetasizer	SEM	EDX

4.3 Characterization of the composite

The phase purity and composition of the synthesized composite powders were analyzed by powder X-ray diffractometry using a Philips X'pert Pro diffractometer working at 45 kV and 20 mA Cu K_α radiation. The phase analyses on the collected X-ray data were achieved by using the built-in computer software of the X-ray diffractometer. The samples were investigated for their microstructure and morphology by using a Philips XL-30S FEG scanning electron microscope. Semiquantitative phase analyses were performed by using the energy dispersive X-ray spectroscopy analyzer equipped in SEM. Size distribution of the particles were obtained from Malvern Zetasizer 3000HSA. Density measurements were done using Archimedes' test apparatus. Compression testing was done on uniaxially pressed samples having dimensions of 15 mm diameter and 20 mm length using a Shimadzu AG-I testing machine.

CHAPTER 5

RESULTS AND DISCUSSION

5.1 Composites Prepared by Wet Mixing of Components

Twelve samples for each of three hydroxyapatite compositions from 30 volume percent to 50 and 70 volume percent were examined for changes in the microstructure, density and sinterability with varying zirconia and alumina content. The variations in hydroxyapatite and TZ-3Y content exhibited a difference in sinterability of the samples and porosity of the sintered bulk material. As seen in Table 13 an increase in hydroxyapatite content corresponds to an increase in density of the samples especially at high temperatures. The increase in density is considered to be due to increase in the homogeneity in the matrix phase and the lower sintering temperature of hydroxyapatite. With increase in temperature other phases contribute to the increase in density by enhanced sintering.

Table 13. Density of wet mixed composites of varying compositions

	30v% HA-70v% AZ			50v%HA-50v% AZ			70v%HA-30v% AZ		
	63-07	56-14	49-21	45-5	40-10	35-15	27-3	24-6	21-9
Density at sintering T (% Th)	1	2	3	4	5	6	7	8	9
1100°	54,32	55,09	53,91	52,92	55,49	52,37	56,31	55,24	53,56
1200°	55,81	60,14	57,10	57,08	61,42	57,47	57,24	56,01	58,07
1250°	55,68	57,11	58,59	57,08	58,87	58,73	61,68	59,09	60,66
1300°	57,46	55,28	61,13	63,29	66,77	68,49	81,17	77,31	70,71

XRD graphs of samples sintered at five different temperatures reveal phase decomposition of hydroxyapatite above sintering temperatures of 1150 °C (Figures 7-11). Beta-tricalcium phosphate formation is seen to be more pronounced with increased zirconia content and higher hydroxyapatite addition. It can be deduced that decomposition of hydroxyapatite is accelerated by the increased presence of zirconia. Increased alumina amount is parallel with reduction in HA decomposition which may be due to increased phase seperation of zirconia and hydroxyapatite. The sample sets

with less than 10 v% TZ-3Y (7-8-9) give the best values for densification, sinterability, crystallinity and phase purity.

Commercial TZ-3Y powder with average particle size less than 180nm, commercial alpha-alumina with particle size around 200 nm, and commercial hydroxyapatite with particle size 200 nm were used. The average particle size is obtained from SEM images as less than 500 nm (Figures 12-13). The particles bonded to each other during sintering to form a matrix of hydroxyapatite dispersed with alumina and zirconia particles (Figures 14-15).

The dependence of composite microstructure on temperature was related to the type of the matrix phase. When the alumina composition was higher (samples 1-2-3) the pores in the microstructure showed an increase in average size and interconnectivity as seen in Figures 13 and 14. When hydroxyapatite was the major phase constituting the matrix, the microstructure as seen in Figure 15 was denser due to lower sintering temperature of hydroxyapatite in comparison to alumina. The contrast in the SEM images helps distinguish phases in the microstructure. The bright grains are assumed to be zirconia phase.

From these wet mixing syntheses 10-20-70 volume percent zirconia-alumina-hydroxyapatite amount was decided as the optimum concentration for phase purity, densification and sinterability

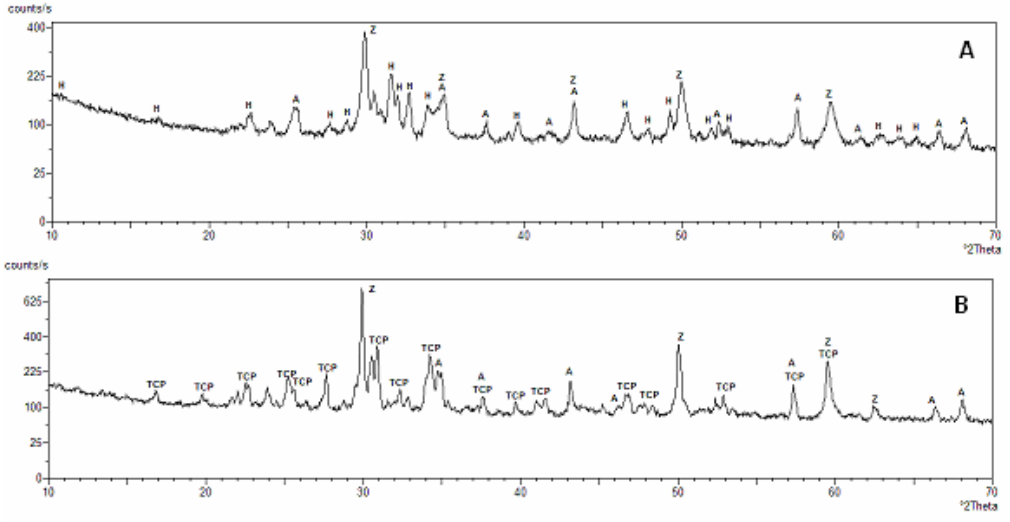

Figure 7. XRD Graphs of 1150 (A) and 1250 °C (B) sintered 10-20-70v% composites (A-alumina, Z-zirconia, H-hydroxyapatite, TCP-beta-tricalcium phosphate)

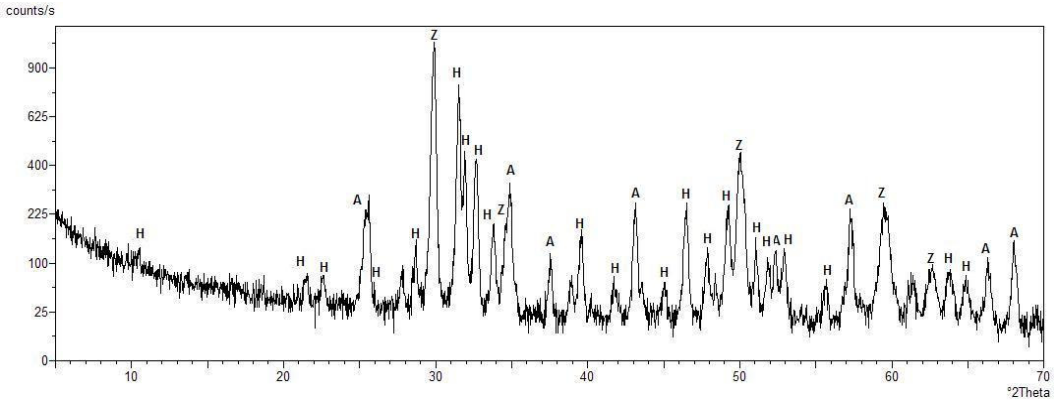

Figure 8. XRD graph of 1100 °C sintered 9-21-70 volume percent composite

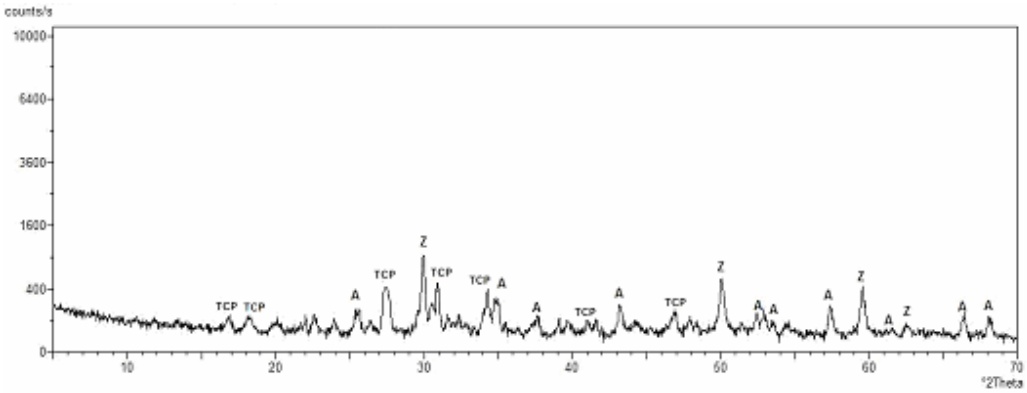

Figure 9. XRD graph of 1200 °C sintered 6-24-70 volume percent composite

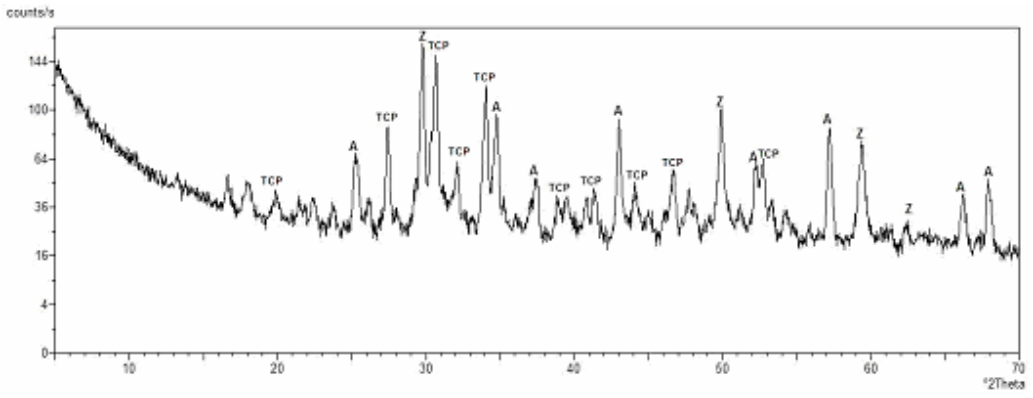

Figure 10. XRD graph of 1250 °C sintered 3-27-70 volume percent composite

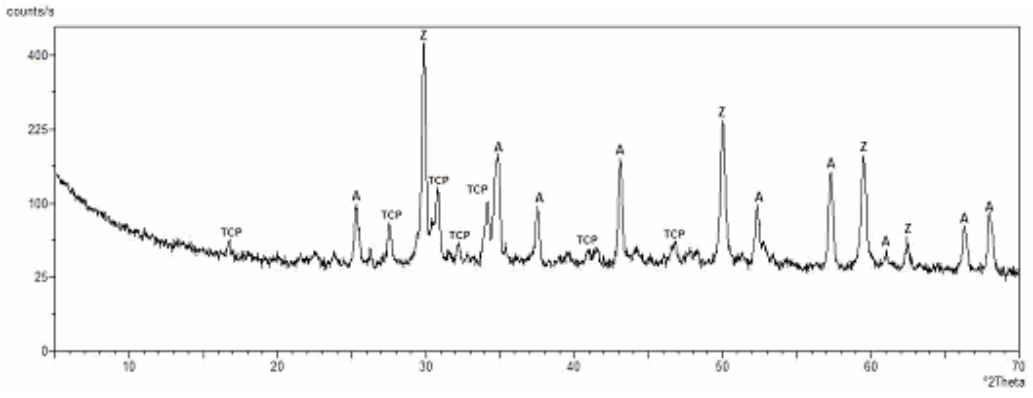

Figure 11. XRD graph of 1300 °C sintered 10-40-50 volume percent composite

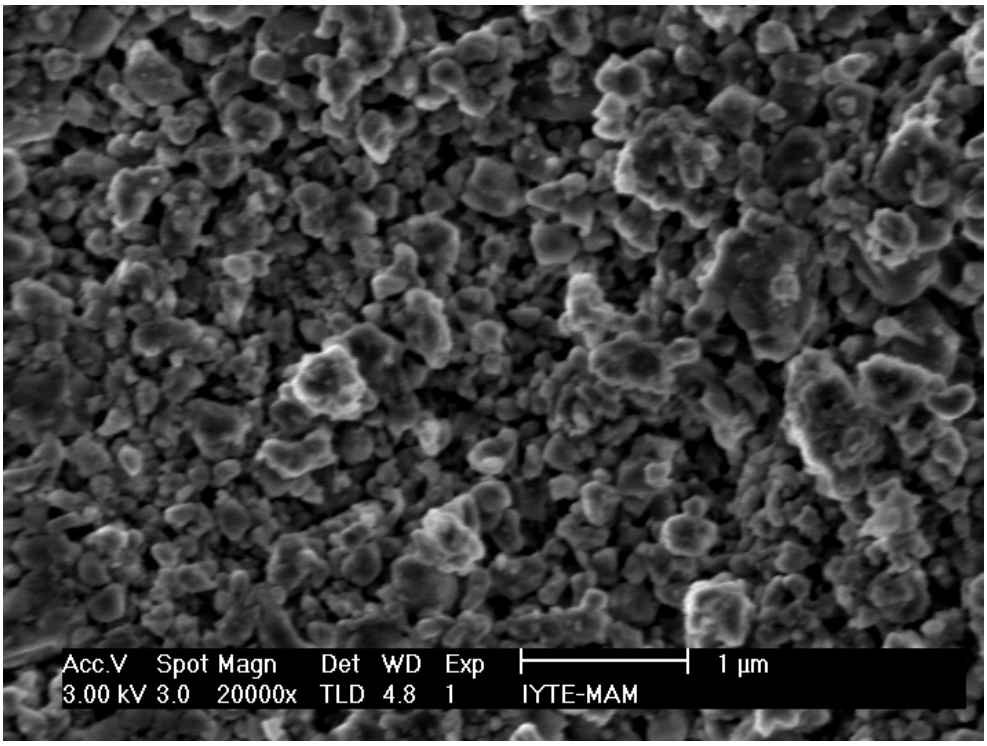

Figure 12. SEM image of 1100 °C sintered wet mixed 15-35-50 volume percent composite

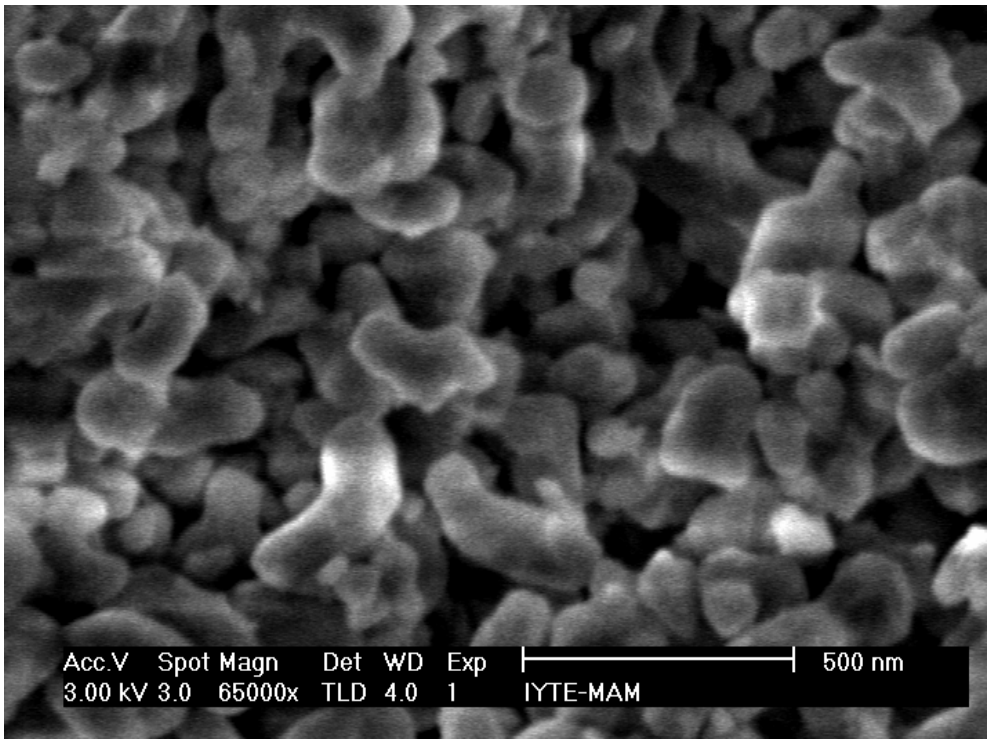

Figure 13. SEM image of 1100 °C sintered wet mixed 7-63-30 volume percent composite

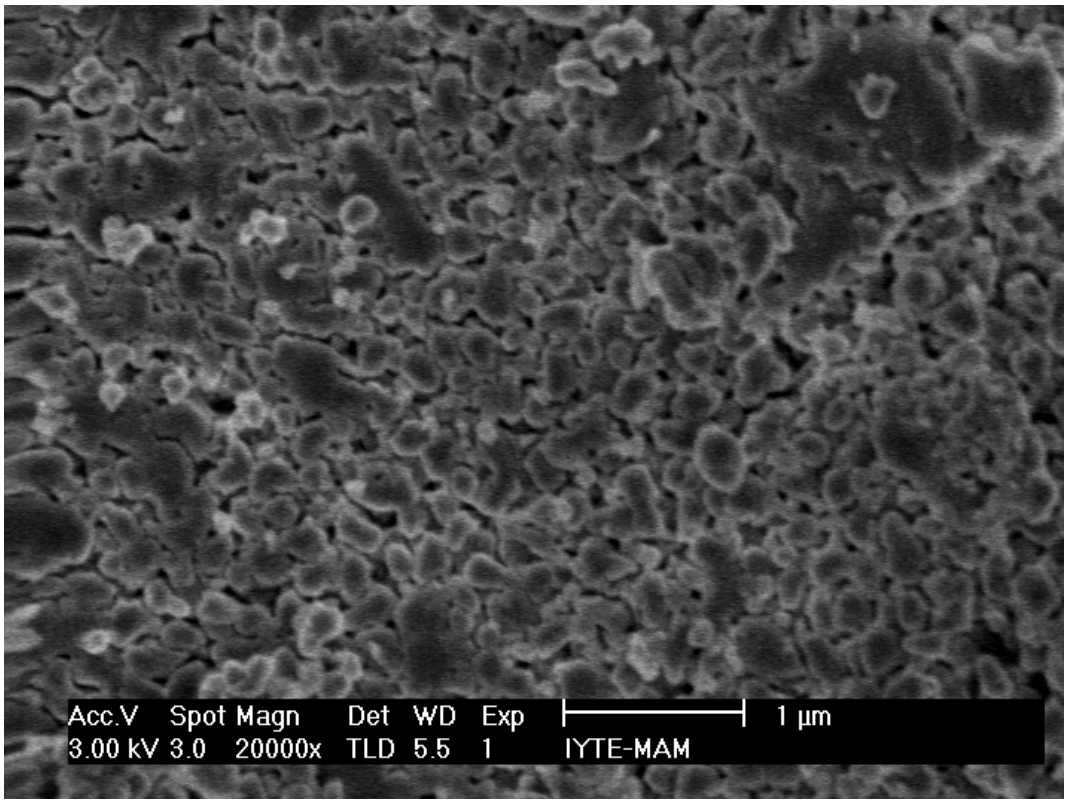

Figure 14. SEM image of 1200 °C sintered 14-56-30 volume percent composite

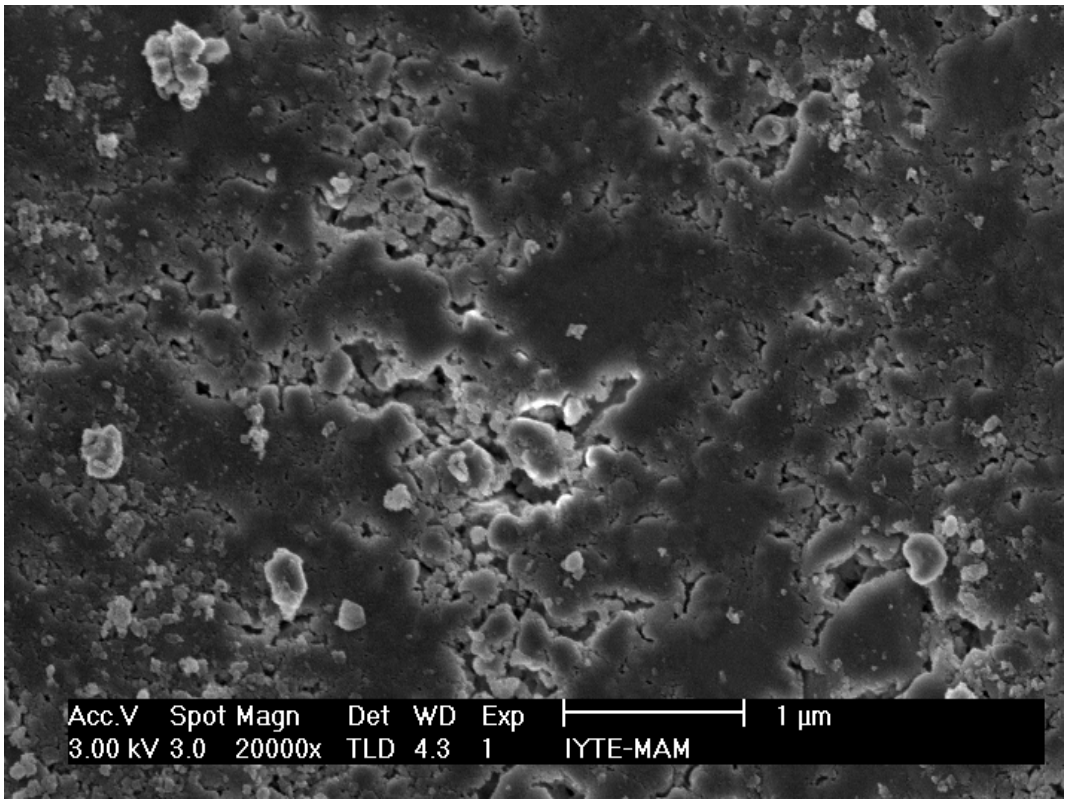

Figure 15. SEM image of 1200 °C sintered 10-40-50 volume percent composite

5.2 Urea Precipitation Method

Heterogeneous precipitation method was applied to the synthesis of alumina coated zirconia cores and HA coated alumina-zirconia nanocomposites using urea as the precipitation agent. In this method the hydroxyl ions released by decomposed urea react with Al^{2+} ions to form boehmite on the surface of the TZ-3Y cores. For complete coating of the added alumina precursor, urea decomposition should take place homogeneously for the necessary amount of time. Therefore urea concentration, precipitation temperature and duration are important variables which determine the success of the coating process.

5.2.1 Composite Particle Model

Developing a theoretical particle model for core-shell structure composite synthesis using the above mentioned precipitation routes aids in setting a criteria for successful synthesis. In the case of a complete coating, homogeneous distribution of coated layers around core in a perfectly spherical particle can be assumed as an ideal product as schematically given in Figure 16 with the corresponding radii calculated for the three phases forming the biocomposite according to the 10:20:70 volume ratio. Comparing this model with the characterized powder products of each synthesis, it is possible to evaluate the syntheses as suitable or not. Based on this assumption the minimum particle size for alumina-zirconia composite particles is calculated as 260nm and for the HA-alumina-zirconia composite particles as 400nm according to the desired 10:20:70 volume ratio. The average size of the core zirconia particles is assumed to be 180nm for this calculation. The molar ratio of alumina to zirconia and hydroxyapatite to zirconia in completely coated particles prepared according to the 10:20:70 volume ratio are calculated as 1.6 and 4.58 respectively. The theoretical density of the composite for this specific ratio is 3.6. Results from particle size characterization with SEM or Zetasizer were compared to these minimum values and the syntheses that produced particles with higher average sizes were considered to yield satisfactory coatings on the previous core phase.

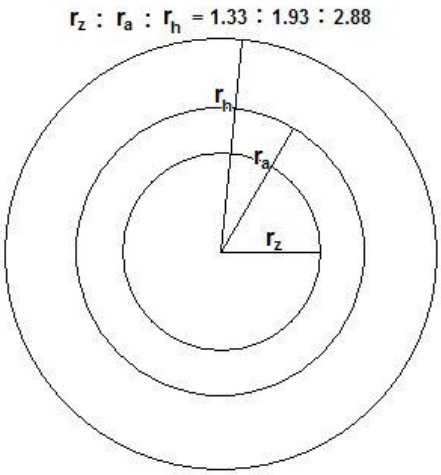

Figure 16. Spherical Particle Model

6.2.2 Alumina Coating on Zirconia

Samples with varying aluminum sulfate/zirconia and urea/aluminum sulfate molar ratios were produced. Aluminum sulfate was mixed with TZ-3Y in ratios from 1.6, which corresponds to the 10:20:70 volume percent ratio, to 8/1. The urea concentration varied between 3 to 12 times aluminum sulfate mole content. The particle size and morphology, elemental analysis, size distribution analysis results were observed for the determination of optimum urea content and processing time. The coated samples had varying average particle sizes that is a result of variation of aluminum sulfate and urea concentration from optimum concentrations. For perfect spherical particle composite with alumina-zirconia volume ratio 10:20 the theoretical particle size is 260nm which is considered the lower limit for the samples. Zetasizer readings and the compositional ratios of the samples are given in Table 14. Zetasizer analyses were done on diluted sample suspensions ultrasonically treated to eliminate agglomerations. EDX elemental analysis results were obtained by taking the average of elemental compositions of five particles for each sample. Based on the average particle sizes AZ2, AZ4, AZ7, AZ15, AZ24, AZ25 were determined as well coated samples.

The relation between stirring time and coating thickness was evaluated by applying 4 different stirring times to samples AZ8, AZ9, AZ10, AZ11 from 2 hours to 5 hours. The particle sizes show increase as expected with increased stirring duration. At 2 hours stirring 150nm particle size is obtained which indicates very thin coating layer.

This value was gradually increased above 260nm by increasing the stirring time to 5 hours. The sufficient stirring time was accepted as 6 hours for the rest of the precipitation experiments.

Table 14. Alumina coated zirconia samples prepared with varying compositions

Urea Alumina Coatings on TZ-3Y					
Sample	$Al_2(SO_4)$/Zirconia	Urea/ $Al_2(SO_4)$	Stirring Duration	Average Particle Size	EDX Al/Zr
AZ1	2/1	3	6h	180nm	55/15
AZ2	4/1	6	6h	500nm	30/3
AZ3	4/1	12	6h	4000nm	
AZ4	4/1	3	6h	250-900nm	42/4
AZ5	4/1	12	6h	900nm	
AZ6	8/1	3	6h	175-750nm	
AZ7	2/1	6	6h	160-550nm	30/16
AZ8	4/1	6	5h	260-1200nm	
AZ9	4/1	6	4h	230-1400nm	
AZ10	4/1	6	3h	200nm	
AZ11	4/1	6	2h	150nm	
AZ15	1.6	10	6h	600nm	26/7
AZ21	4/1	6	6h		28/4
AZ22	1.6	10	6h		35/3
AZ24	4/1	10	6h	260nm	20/2
AZ25	1.6	6	6h	600nm	18/9

$Al_2(SO_4)$/Zirconia ratio and urea/$Al_2(SO_4)$ ratio both have effects on average coating thickness. While low urea/$Al_2(SO_4)$ results in thin coating layer(AZ1, AZ4, AZ6), low $Al_2(SO_4)$/Zirconia has effect of decreasing the aluminum volume content relative to zirconium (AZ1, AZ7). Bimodal particle size distribution is obtained at nearly half of the low urea/$Al_2(SO_4)$ samples irrespective of $Al_2(SO_4)$/Zirconia ratio and narrow size distribution is seen with high urea/$Al_2(SO_4)$ ratio. This may be the result of insufficient urea decomposition and its effect on formation of agglomerates by the prolonged attachment step of aluminum ions on multiple zirconia cores. In order to keep the alumina/zirconia ratio at the optimum level of 10:20 volume percent and obtain a narrow size distribution, combination of low $Al_2(SO_4)$/Zirconia and high urea/$Al_2(SO_4)$ is used.

The decomposition of urea in the presence of aluminum sulfate proceeds through the following reactions:

$$(NH_2)_2CO+3H_2O \rightarrow 2NH_4^+ + CO_2 + 2OH^- \quad (1)$$

$$Al_2(SO_4)_3+4(NH_2)_2CO +(x+7)H_2O \rightarrow Al_2O_3 \cdot xH_2O+3(NH_4)_2SO_4+2NH_3+4CO_2 \quad (2)$$

At temperatures exceeding the decomposition temperature of urea, 85 °C, continous supply of hydroxyl ions is provided in the reaction medium until total decomposition of urea . Hydroxyl ions are consumed by the dissolved aluminum ions and aid in forming a boehmite precipitate around the equiaxed core zirconia particles. As the average particle size of zirconia cores is small (<180 nm) theoretically metal cations deposit on the cores in a short period of time and further deposition occurs at random nucleation sites on the same boehmite layer so the composite particles may have shape with preferred orientation instead of equiaxed spherical particles. Parameters of the precipitation process like stirring rate and time, temperature of the medium are highly influential on precipitation mechanism, phase stability and coating morphology.

The average particle size of AZ2 from zetasizer characterization is in agreement with the SEM image shown in Figure 17. Equiaxed particles consisting of small agglomerates of boehmite coated zirconia particles that are greater than 250nm can be observed in the same image.

Equiaxed particles of AZ15 were similar to AZ2 particles in morphology with uniform size distribution. This powder sample consisted of small agglomerates of spherical particles that are about 1 micron in size as shown in Figure 18. Uniform coating under homogeneous stirring conditions has been obtained around zirconia cores due to use of high urea/$Al_2(SO_4)$ for the stoichiometric $Al_2(SO_4)$/zirconia. The particle size exceeding the expected size is indicative the effect of high urea concentration on increasing particle size.

The SEM micrograph given in Figure 19 indicates the presence of equiaxed particles consisting of agglomerates of particles less than 500nm in diameter for AZ4. The difference of half urea/$Al_2(SO_4)$ of AZ4 from AZ2 results in higher particle size due to higher amount of agglomerates. Numerous agglomerates of small particles of AZ7 have particle sizes close to 500 nm. Bimodal particle size distribution obtained by the zetasizer analysis is indicative of bonding between separately coated particles with a boehmite layer due to combination of low $Al_2(SO_4)$/zirconia and urea/$Al_2(SO_4)$ as is evident in Figure 20.

AZ24 and AZ25 contain particles of spherical morphology having particle size around 500 nm. Uniform size distribution of AZ24 as seen in Figure 21 is consistent with the high urea/$Al_2(SO_4)$ use and the agglomerations in AZ25 causing a bimodal distribution of particles is a result of combination of low $Al_2(SO_4)$/zirconia and urea/$Al_2(SO_4)$ used.(Figures 22)

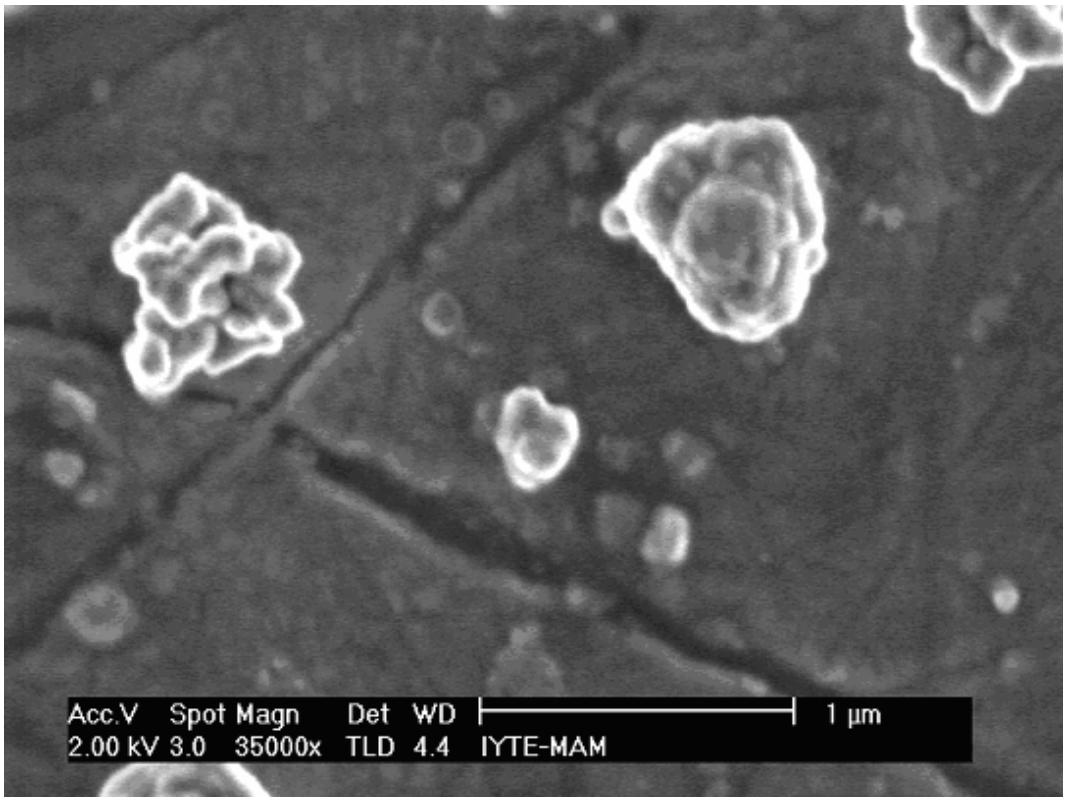

Figure 17. SEM image of AZ2

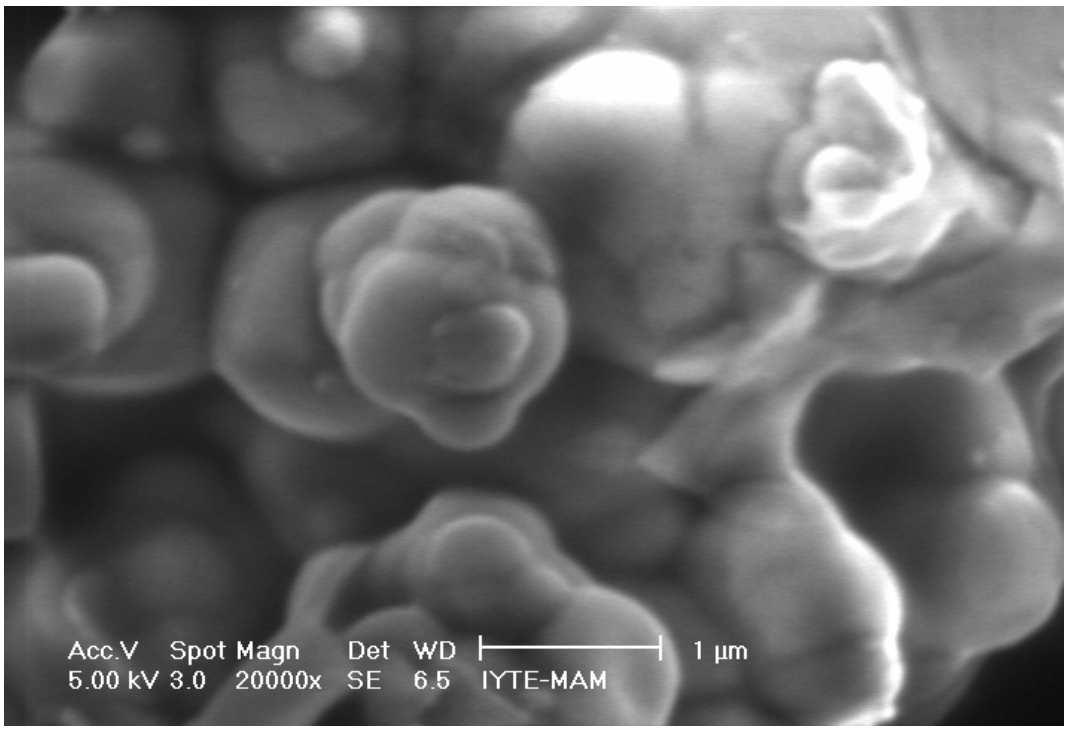

Figure 18. SEM image of AZ15

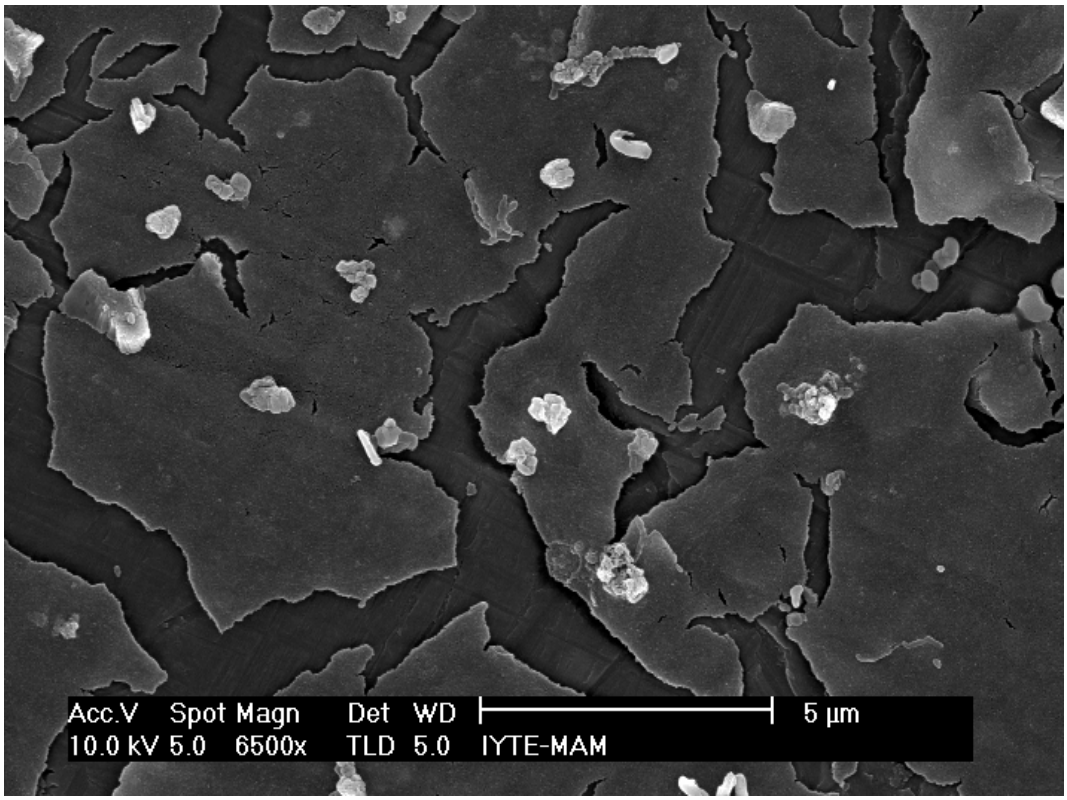

Figure 19. SEM image of AZ4

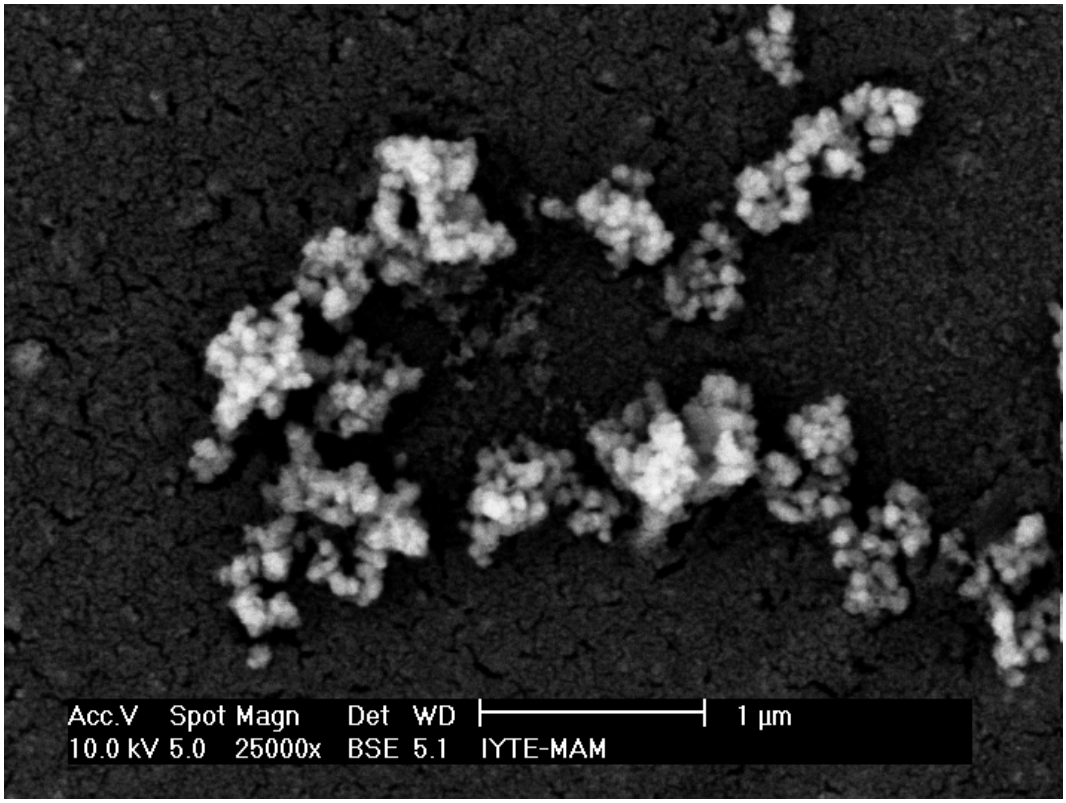

Figure 20. SEM image of AZ7

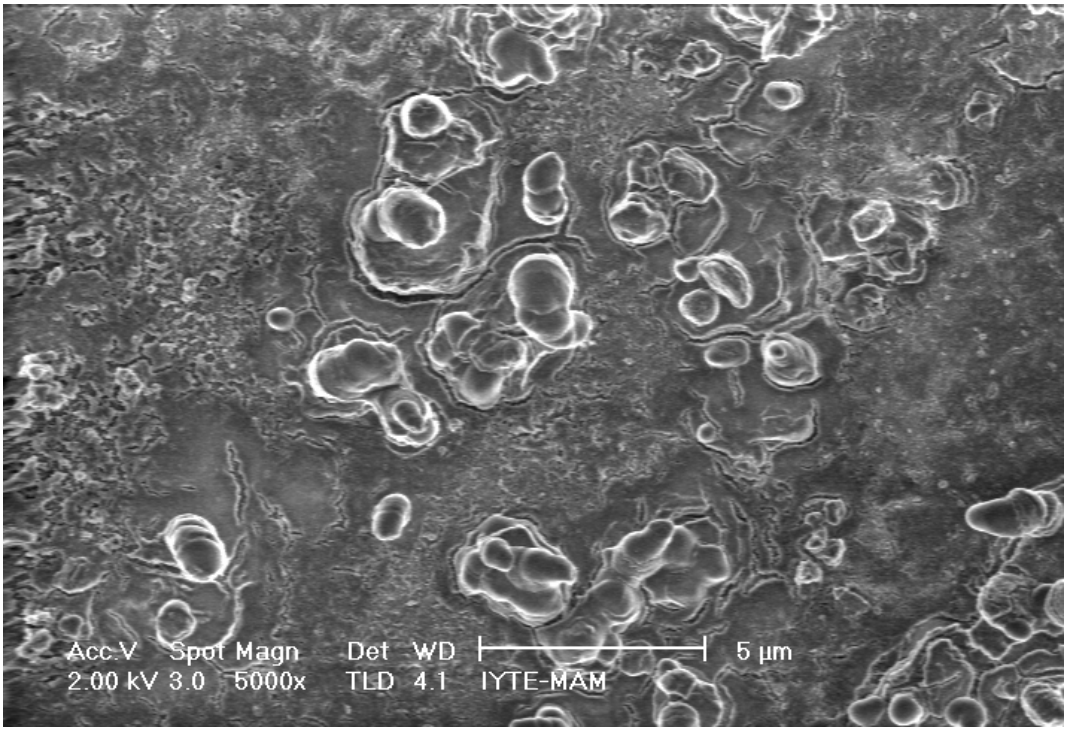

Figure 21. SEM image of AZ24

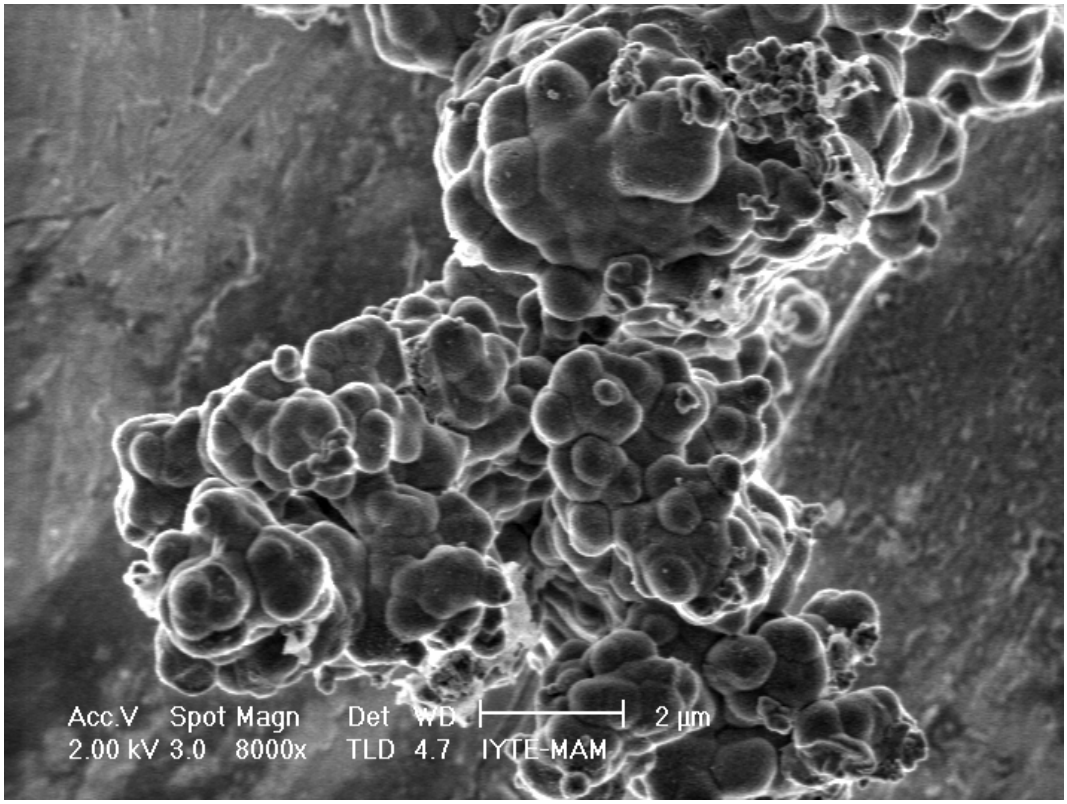

Figure 22. SEM image of AZ25

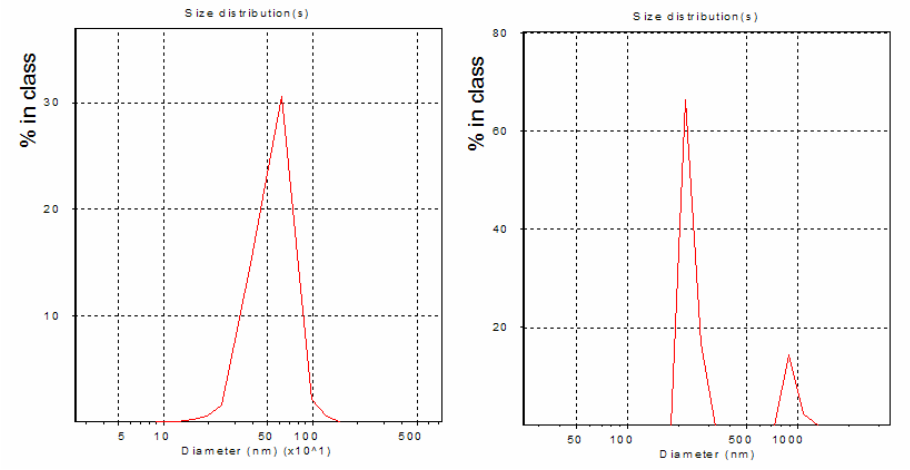

Figure 23. Size distribution graphs of AZ2, AZ4 respectively

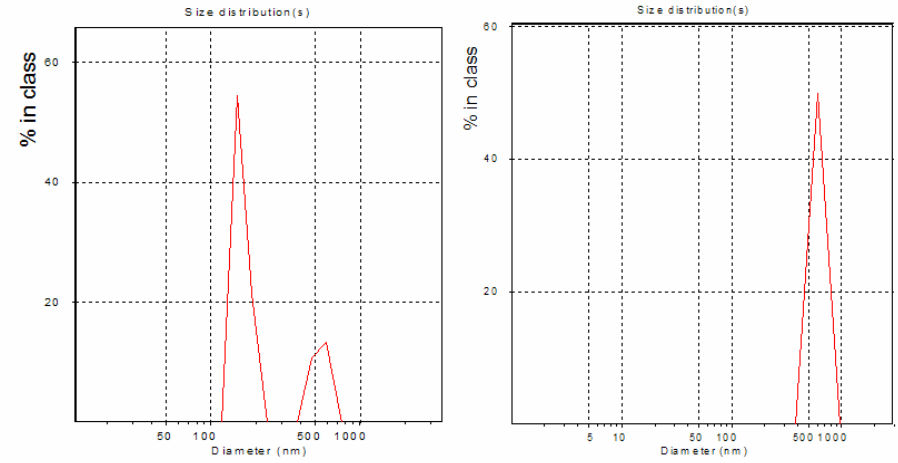

Figure 24. Size distribution graphs of AZ7, AZ15 respectively

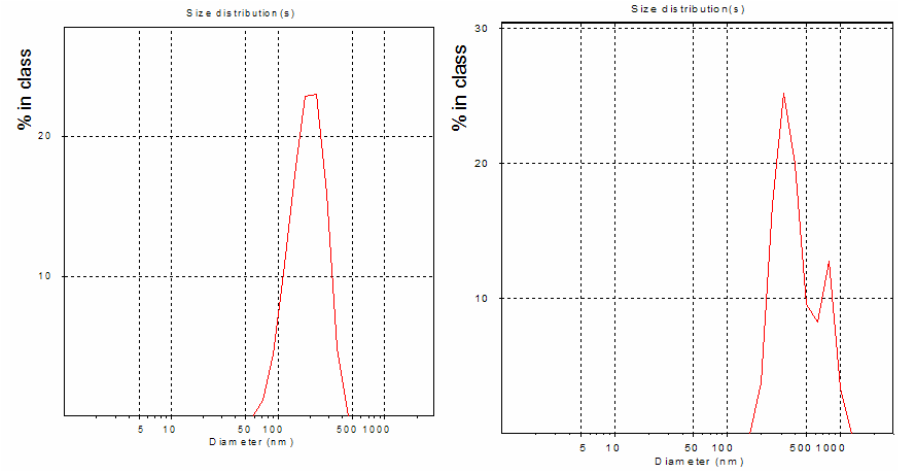

Figure 25. Size distribution graphs of AZ24, AZ25 respectively

Size distribution intensity graphs for zetasizer analysis seen in Figures 23 and 24 give bimodal distribution for the samples AZ4 and AZ7. One group of particles below the lower coating limit of 260nm and other group around 1 micron indicates agglomerated coatings of boehmite on multiple zirconia particles and lack of homogeneous attachment of boehmite. This may be due to lower availability of aluminum ions around zirconia or less amount of precipitated aluminum ions at local sites due to insufficient urea decomposition. Samples AZ2 and AZ15 have uniform distribution of particles >500nm in agreement with SEM observations. AZ24 particles are at the lower coating limit with a narrow size distribution indicating well coating. Sample AZ25 has a wide distribution of particles between lower limit and 1 micron size as seen in Figure 25 that may be caused by excessive agglomeration.

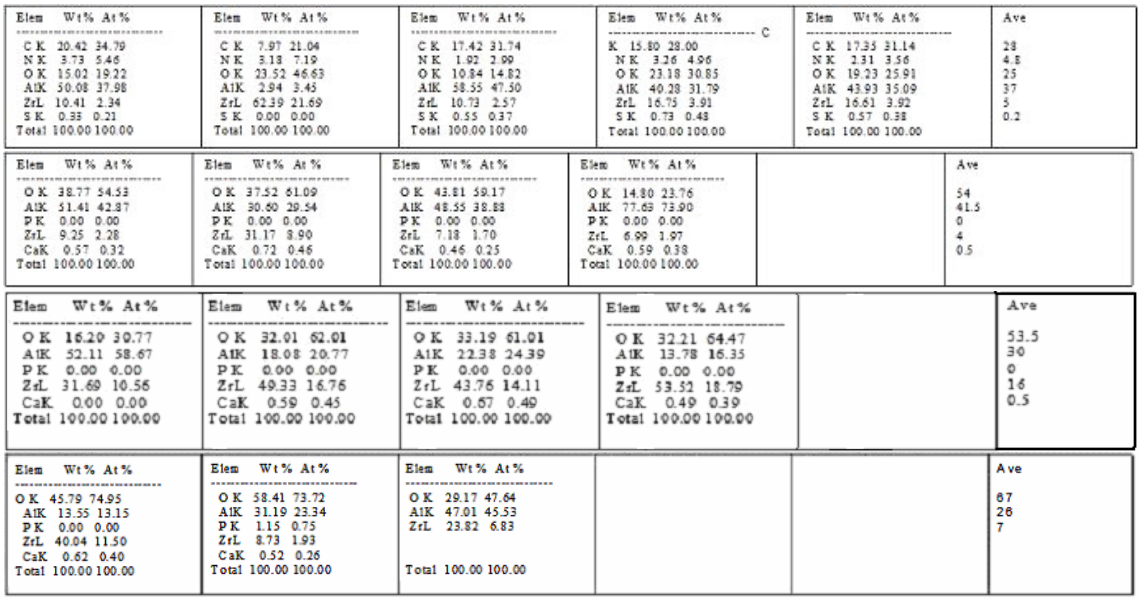

Figure 26. EDX analyses of samples AZ2, AZ4, AZ7, AZ15 respectively

Compositional analysis reveals all samples contain a boehmite phase in uncalcined state in varying amounts. The aluminum/zirconium amount for completely coated theoretical 10:20 volume ratio spherical particle is calculated as 3.2 for atomic ratio. This ratio in the EDX analysis results indicates sufficient and successful coating. Comparison between the Al/Zr ratio of precursors for the samples and the corresponding EDX ratios gives efficiency of the coating process and hence the effect of urea concentration.

AZ2 $Al_2(SO_4)/ZrO_2$=4/1 Urea/$Al_2(SO_4)$=6 EDX Al/Zr=37/5 > 3.2 sufficient coating

AZ4 $Al_2(SO_4)/ZrO_2$=4/1 Urea/$Al_2(SO_4)$=3 EDX Al/Zr=42/4 > 3.2 sufficient coating

AZ7 $Al_2(SO_4)/ZrO_2$=2/1 Urea/$Al_2(SO_4)$=6 EDX Al/Zr=30/16< 3.2 insufficient coating

AZ15 $Al_2(SO_4)/ZrO_2$=1.6 Urea/$Al_2(SO_4)$=10 EDX Al/Zr=26/7 > 3.2 sufficient coating

AZ24 $Al_2(SO_4)/ZrO_2$=4/1 Urea/$Al_2(SO_4)$=10 EDX Al/Zr=20/2 > 3.2 sufficient coating

AZ25 $Al_2(SO_4)/ZrO_2$=1.6 Urea/$Al_2(SO_4)$=6 EDX Al/Zr=18/9 < 3.2 insufficient coating

AZ15 is a sample with suitable precursor compositions and particle size, morphology characteristics in comparison with the other five samples for the synthesis of composite cores. Urea/aluminum sulfate or calcium nitrate ratio of 10 is considered the most suitable for both alumina and HA coating based on these EDX and zetasizer characterizations.

Alumina coated samples exhibit different levels of crystallinity of alumina as observed from intensities in the XRD graphs. Broad alumina peaks in comparison with sharp zirconia indicate nucleation and growth of fine boehmite grains with low crystallinity during precipitation process. This may be due to precipitation of the boehmite crystals at low temperatures. The boehmite phase of AZ25 in as synthesized condition and alumina phases of AZ15, AZ21, AZ22 that are calcined at 1050 °C are seen in Figure 27. The low intensity of the broad alumina peaks of AZ15, AZ21, and AZ22 indicates that alumina coating has low crystallinity. The same low crystalline boehmite precipitation is present in uncalcined sample AZ25.

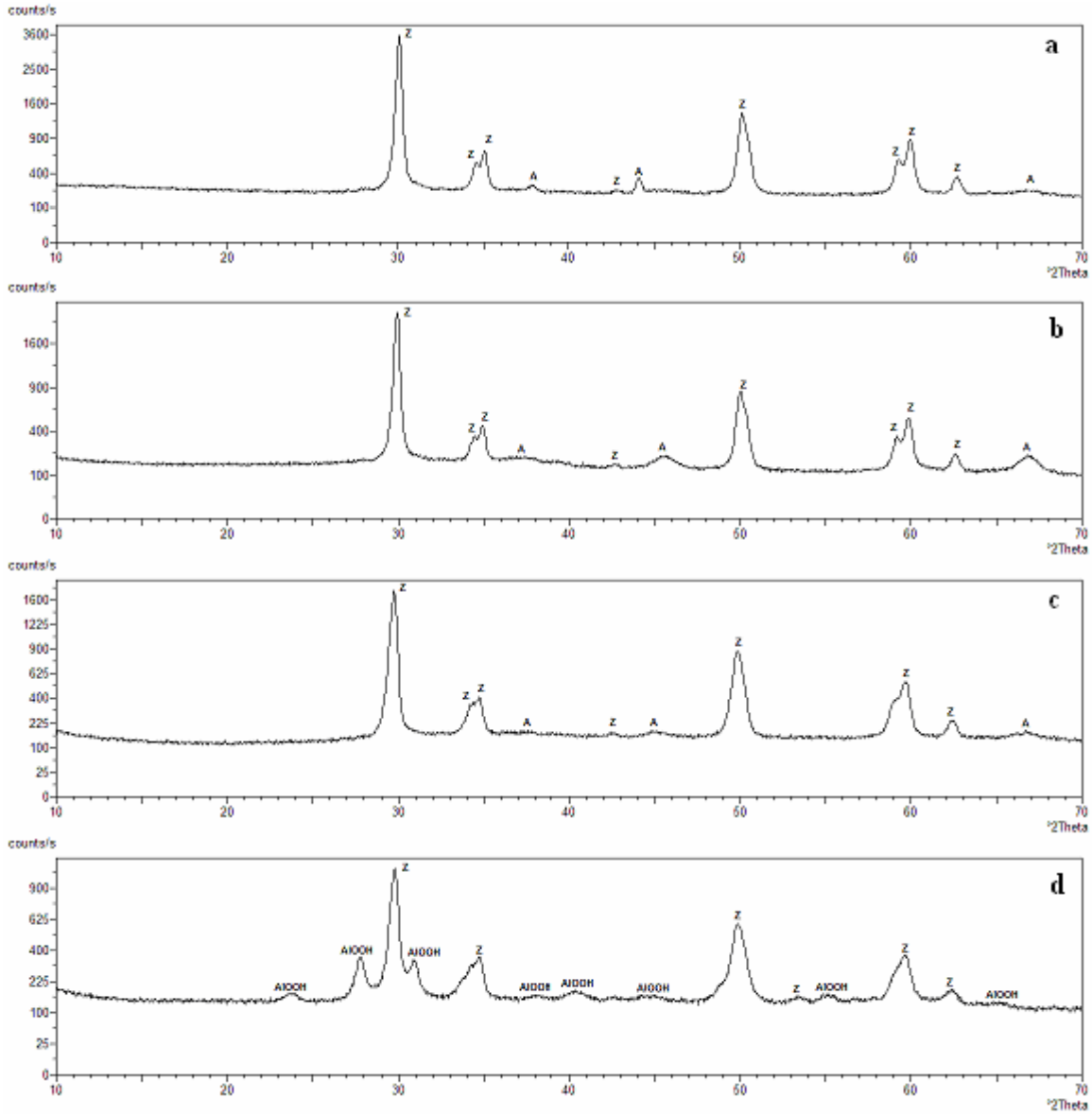

Figure 27. XRD graphs of (a) AZ15, (b) AZ21, (c) AZ22, (d) AZ25 respectively (A-alumina, Z-zirconia, AlOOH-boehmite)

5.2.3. Hydroxyapatite Coated Alumina-Zirconia Cores

Hydroxyapatite coating on alumina coated zirconia cores was applied with stoichiometric amount of calcium and phosphorus precursors calcium nitrate tetrahydrate and ammoniun phosphate using urea as the precipitating agent. For all samples calcium nitrate/ammonium phosphate ratio was set at 1.67, urea ratio to calcium cations was set at 10 and the relative ratio of the alumina-zirconia cores to theoretical hydroxyapatite yield was set at 30/70 by volume for the 10:20:70 volume

percent composite model with assumption that the cores have a zirconia/alumina volume ratio of 10:20. This has been achieved with some samples that have been presented in the report, while the other samples with deviated compositions have still been coated to observe variations in coating process. The average particle size for sufficiently coated spherical three component composite particle is expected to be at least 400nm and the thickness for hydroxyapatite coating layer is expected to be greater than 150nm. In practice HA coated samples with particle size around 1 micron is considered satisfactory.

Table 15. Hydroxyapatite coated composite concentrations and properties

HA coatings on Alumina-Zirconia cores							
	Core	Urea	Ca Nit.	Amm. Phos.	Characterization		
AZH5	0.5 gr AZ5	4.3 gr	1.705gr	0.573 gr	Zetasizer 200-500nm	SEM	EDX Ca18 P12
AZH7	0.1 gr AZ7	1.13 gr	0.446gr	0.115 gr	Zetasizer 1000nm		
AZH10	0.5gr AZ9	4.3 gr	1.705gr	0.573 gr	Zetasizer 950nm	SEM	
AZH18	2.1 gr AZ15	20.6 gr	8.1 gr	2.72 gr	Zetasizer 920nm	SEM	EDX Ca25 P13
AZH19	1gr AZ4	8.6 gr	3.41gr	1.146gr	Zetasizer 650nm	SEM	EDX Ca19 P14
AZH20	0.97gr AZ7	8.4 gr	3.39gr	1.12gr	Zetasizer 850nm	SEM	EDX Ca11 P7.3
AZH22	0.5gr AZ21	4.3gr	1.705gr	0.57gr		SEM	EDX Ca7 P3.5
AZH23	1.04gr AZ22	8.6gr	3.41gr	1.15gr		SEM	EDX Ca9.5 P6.5
AZH25	1.2gr AZ24	8.6gr	4.1gr	1.38gr	Zetasizer 500nm	SEM	EDX Ca15 P9
AZH26	3.33gr AZ25	28.9gr	11.35gr	3.83gr		SEM	EDX Ca12 P8

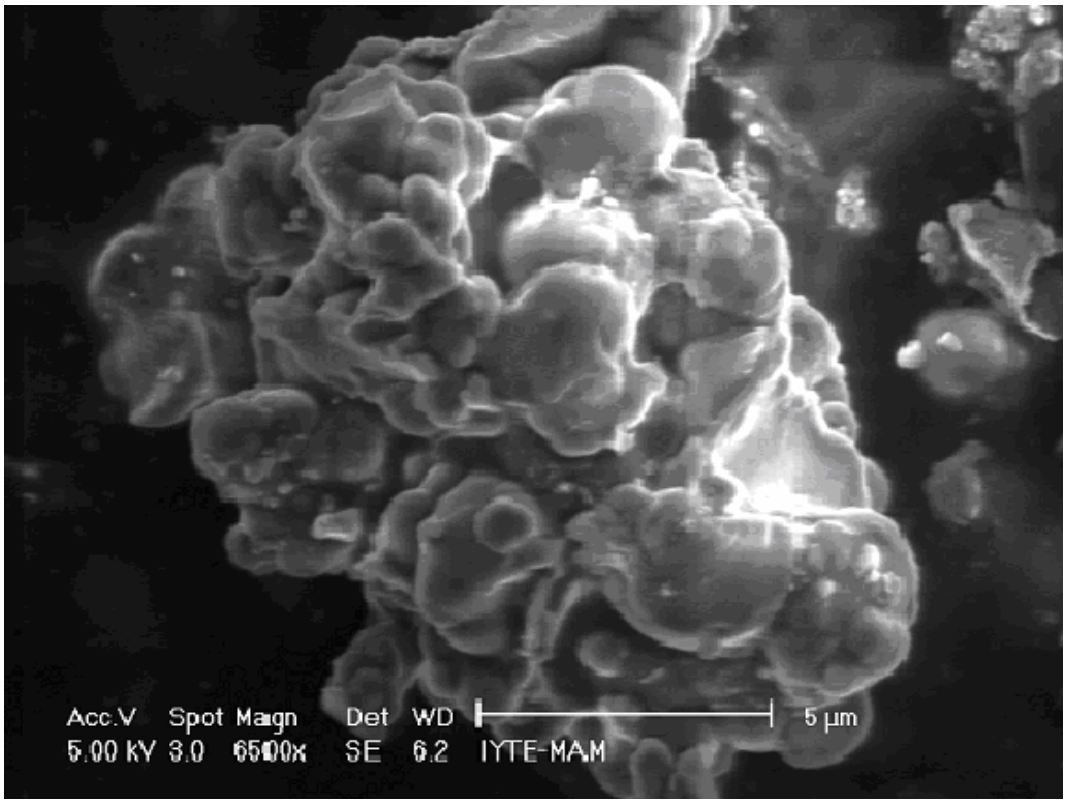

Figure 28. SEM image of HA coated sample AZH18

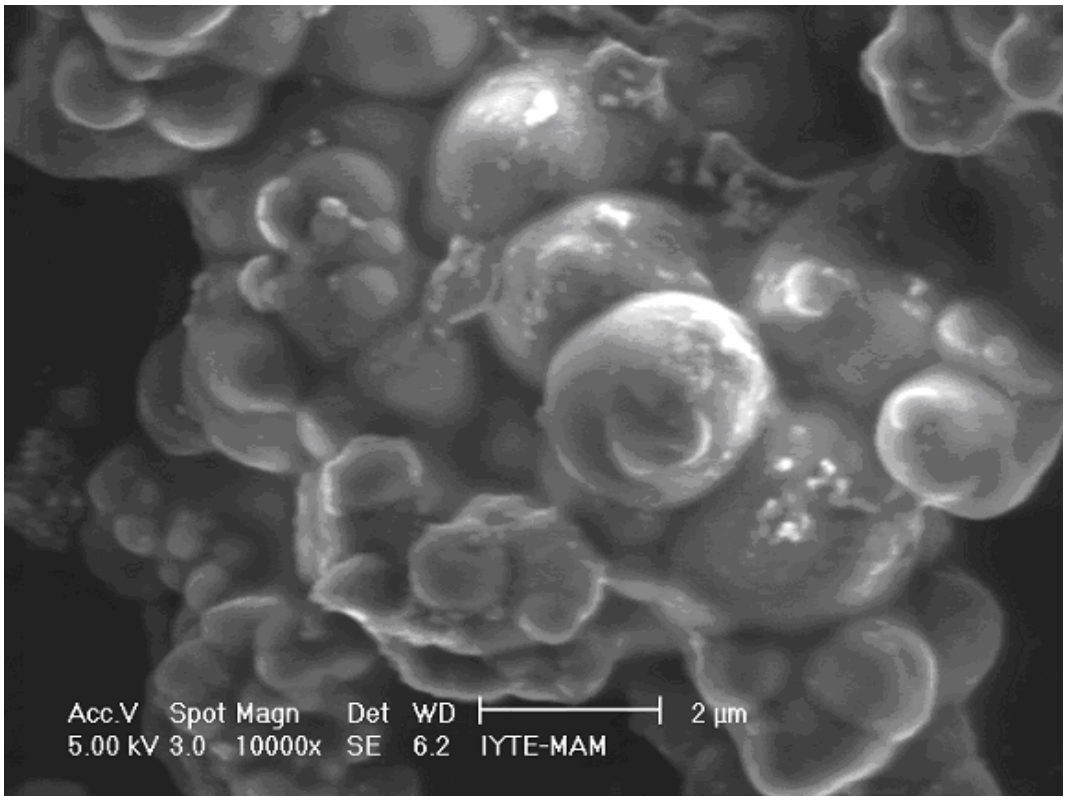

Figure 29. SEM image of HA coated sample AZH18

Hydroxyapatite coated sample AZH18 consists of spherical particles with rounded hydroxyapatite crystals on AZ15 cores. Homogeneously precipitated small round particles are seen in Figures 28-29 with large particles having diameters between 1-2 microns most of which are assumed to be satisfactory heterogeneous coatings on equiaxed AZ15 cores with average particle size of 600nm. Rounded thick hydroxyapatite crystals are known to be precipitated at high temperature so the AZH18 sample is considered to be synthesized at proper stirring and heating conditions with low temperature gradient throughout the precipitation medium. (Lazic et al. 2001) XRD graph of the sample shows intense hydroxyapatite peaks indicating that hydroxyapatite has been precipitated uniformly as the major phase and the calcium and phosphate precursors has been largely consumed.

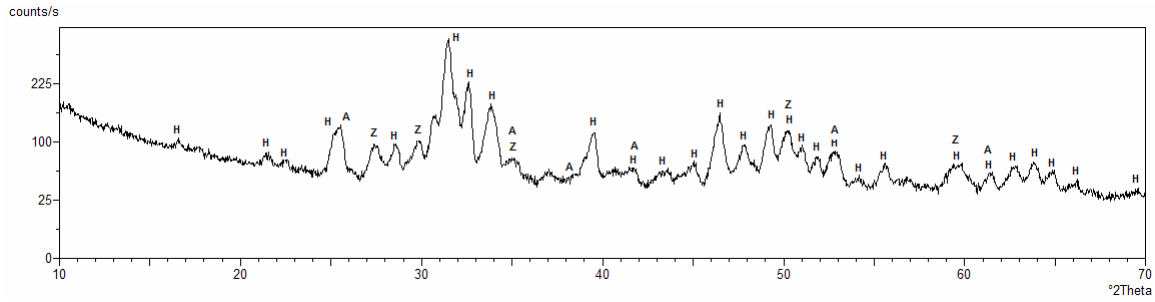

Figure 30. XRD graph of AZH18 sintered at 1050 ° C

AZH19 particles exhibit a thin needle like morphology of hydroxyapatite crystals precipitated on AZ4 cores. EDX results given in Figure 31 show a Ca/P ratio close to stoichiometry and XRD graphs confirm that hydroxyapatite is the stable phase at sintering temperature of 1050°C. The particles are agglomerates of equiaxed hydroxyapatite coated cores as seen in Figures 32 and 33. Thin needle and plate-like hydroxyapatite crystals appear at low synthesis temperatures which indicates temperature was not uniform in the precipitation medium.

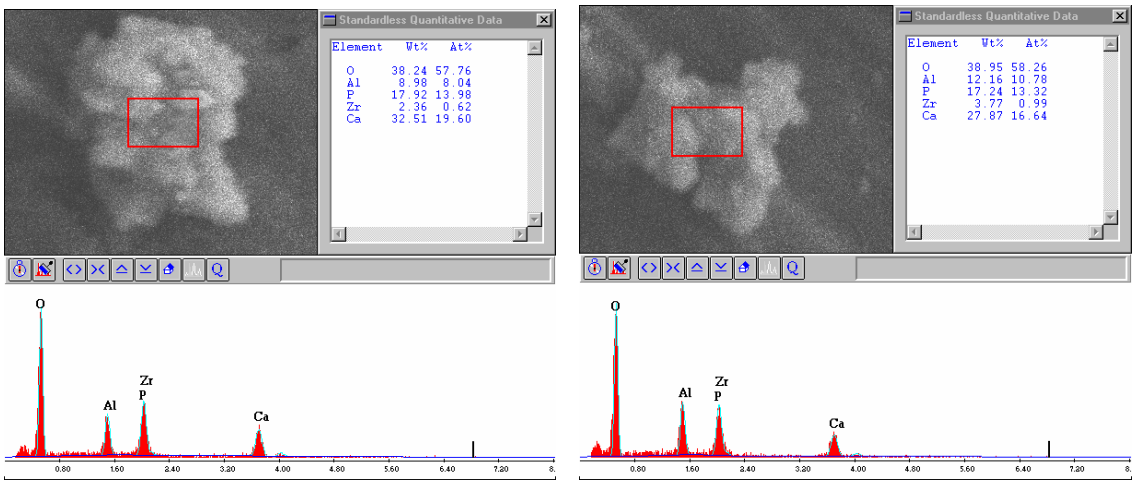

Figure 31. EDX analysis of AZH19 at two different particles

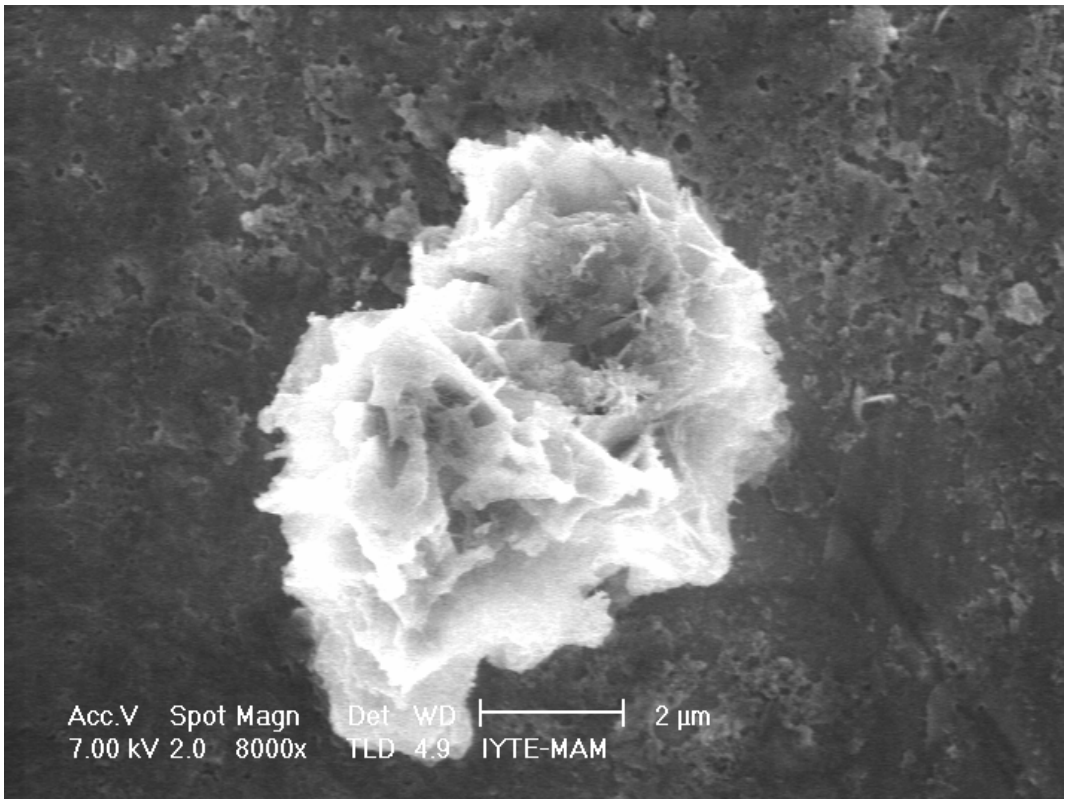

Figure 32. SEM image of AZH19

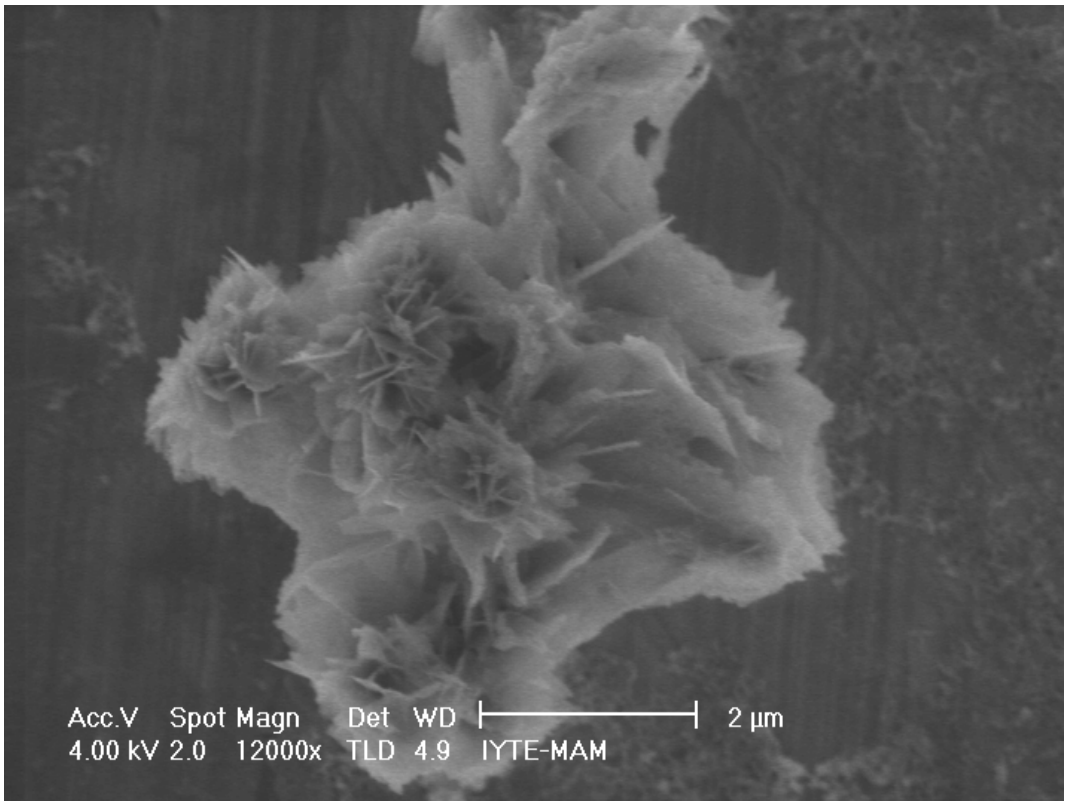

Figure 33. SEM image of AZH19

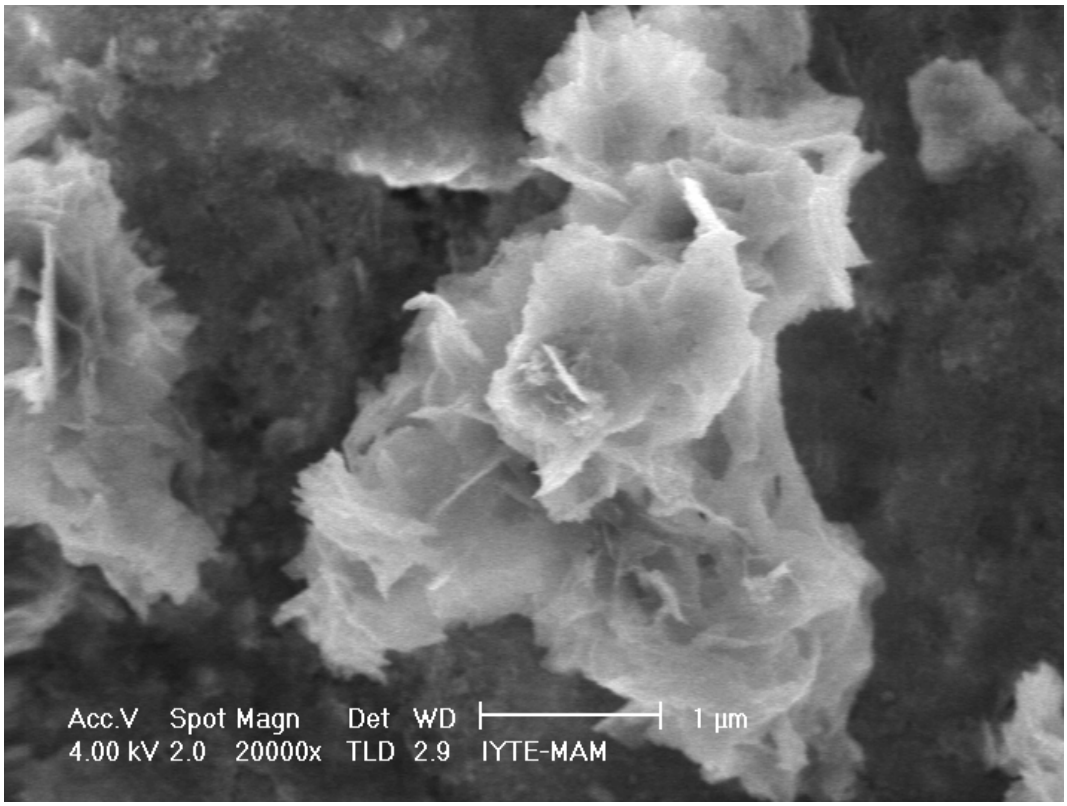

Figure 34. SEM image of AZH20

Particles with average size of about 1 micron have been obtained for AZH20 sample. Figure 34 shows the presence of agglomerates of equiaxed particles and plate like HA formation which were stable even after ultrasonic treatment. The large agglomerate formation was possibly a result of low temperature precipitation that produces the same plate-like crystal morphology. Hydroxyapatite peak intensity of samples with this type of hydroxyapatite structure was lower as given in Figure 35 indicating that a hydroxyapatite coating with a lower crystallinity forms on and between the cores which is responsible for the formation of large agglomerates during low temperature precipitation. A thick hydroxyapatite coating layer around 500 nm is precipitated on AZ7 cores that causes a high level of agglomeration.

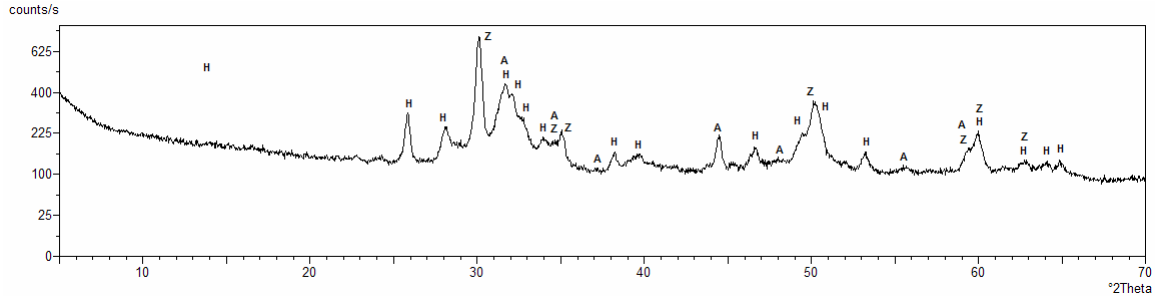

Figure 35. XRD graph of AZH20

The morphology of AZH25 sample is composed of spherical particles with rounded TCP crystals. The presence of some plate-like crystals on the particles indicates the sample had been synthesized in a medium with some temperature gradient major precipitation being completed at high temperature areas of the medium (Figures 36-37). The EDX analysis for the sample gives an average Ca/P ratio of 15/9 which is consistent with beta-tricalcium phosphate formation observed in XRD graph. The particle size measurements from zetasizer analysis and from SEM image indicate ideal core-shell structure is obtained with this sample having average AZ24 core diameter higher than 250 nm and hydroxyapatite coated particle diameter around 500 nm.

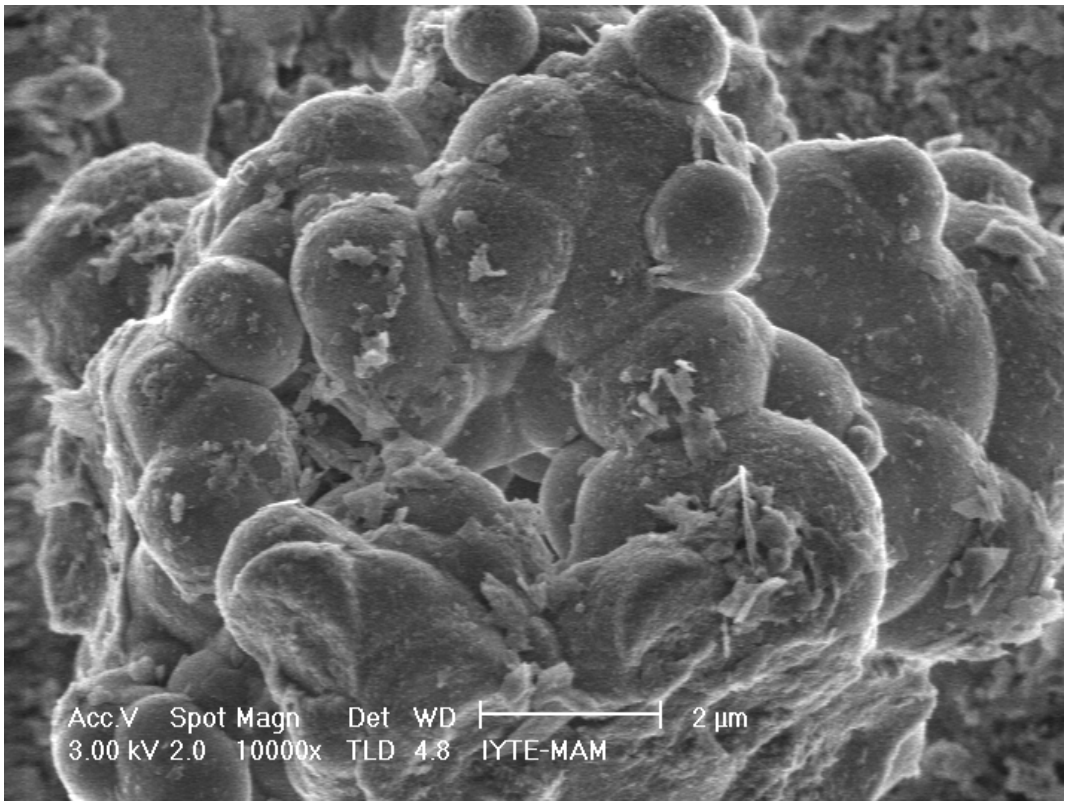

Figure 36. SEM image of AZH25

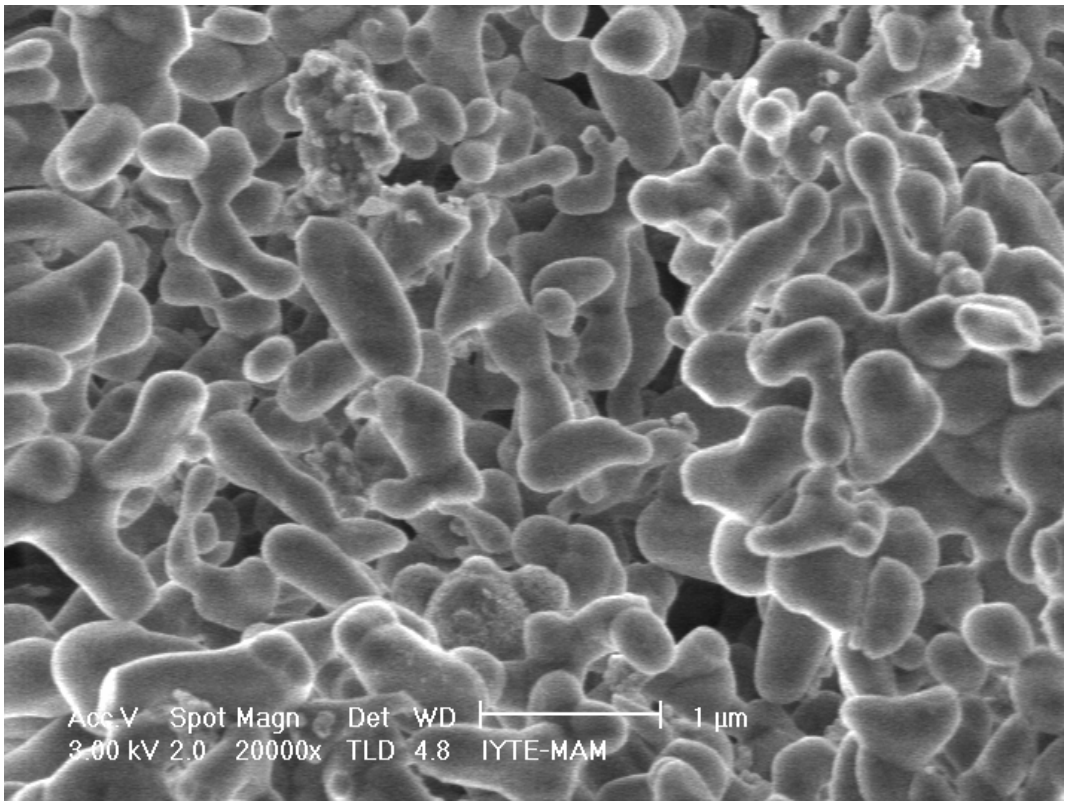

Figure 37. SEM image of AZH25

Composite sample AZH18 has received satisfactory results from all characterization tests including particle size, particle morphology, elemental and phase composition. It has been further characterized for investigation of thermal behavior, bulk microstructure, mechanical properties.

5.3. Morphology of the Composite

AZH18 composite sample has been pressed into pellets and sintered at 1050, 1150, 1250 °C. The fracture surfaces that present similarities with the bulk material has been examined. The fracture surface gives information about the pore size distribution, pore interconnectivity and hence the sinterability of the composite. Pores that occur naturally and with evoluiton of water vapor during sintering has poor interconnectivity and the average pore size is in the region of 10 microns for micro pores that exist between grains with no interconnectivity. Macro pores form channels on the order of 50 microns with low interconnectivity. Low sinterability of the composite is evident from entrapped micro pores around the rigid groups of crystal grains. No phase segregation is observed at the edge and corners of the grain boundaries. The matrix consists of continous hydroxyapatite crystals with alumina and zirconia embedded in the grains. Average grain size is between 1 to 3 microns and a uniform size distribution of grains exist. There is no significant change in pore and grain sizes with increasing sintering temperature. Fracture has occured intergranularly leaving grains with sharp boundaries. The intergranular nature of fracture is clearly seen in Figure 41 as a propogated crack is arrested between the grain boundaries.

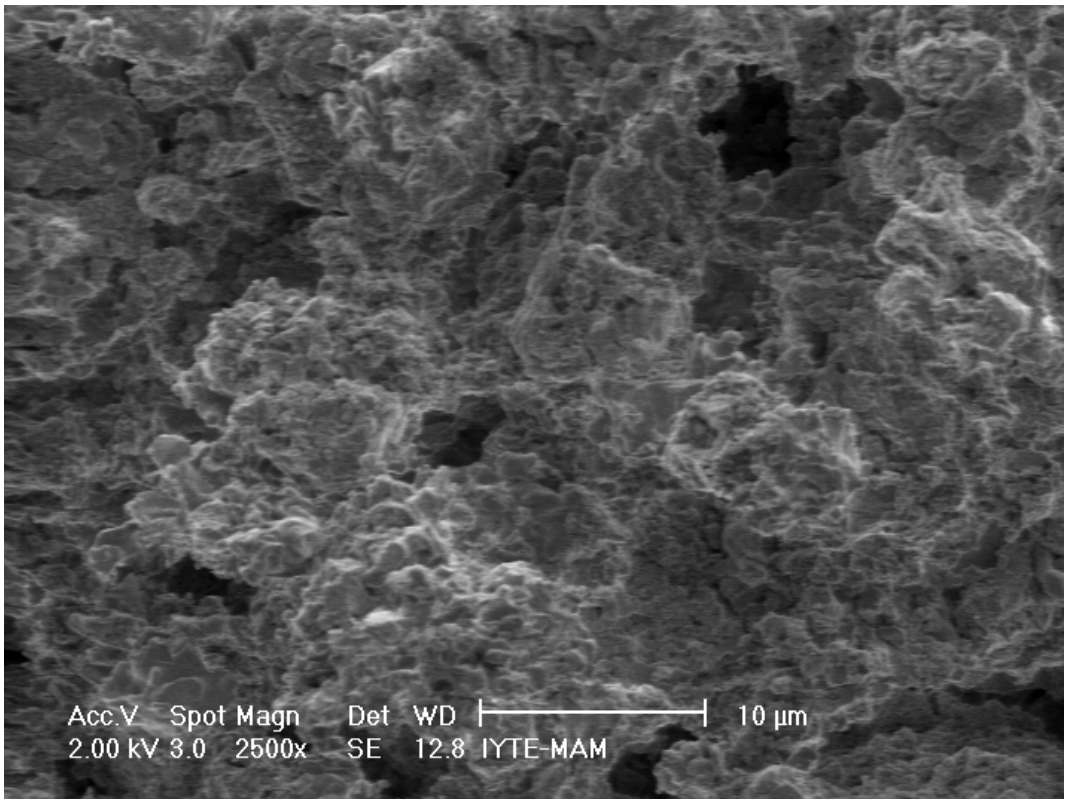

Figure 38. SEM image of 1050 °C sintered composite

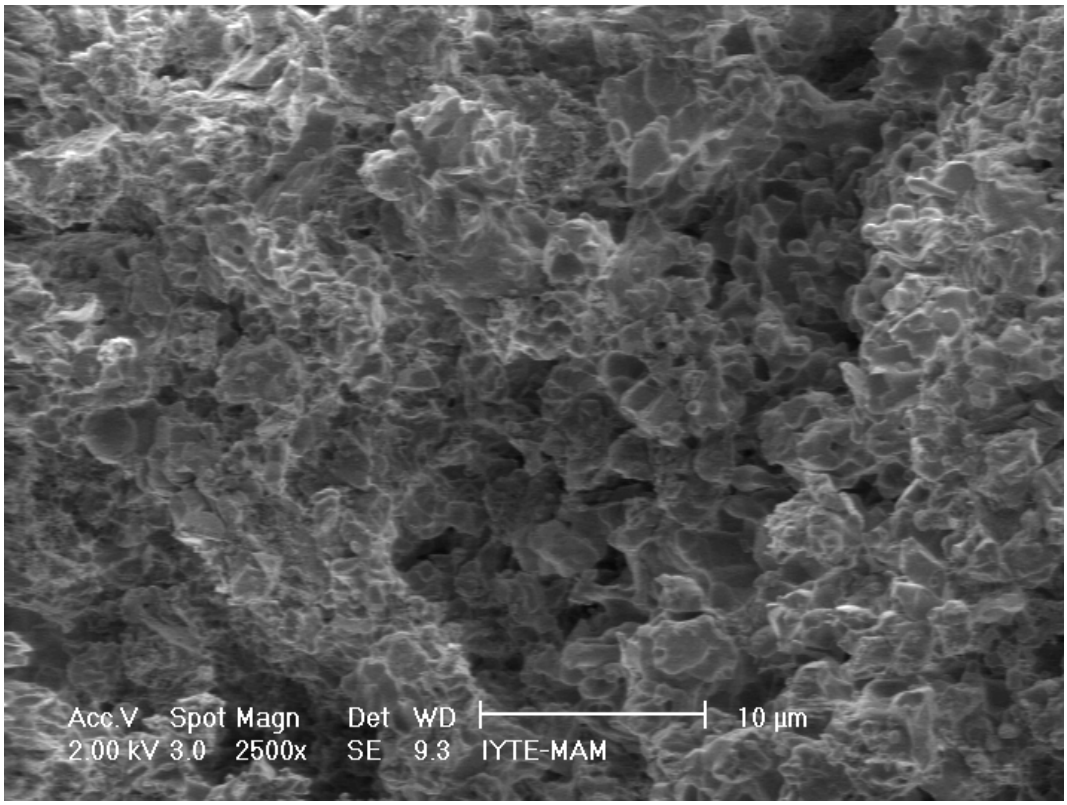

Figure 39. SEM image of 1150 °C sintered composite

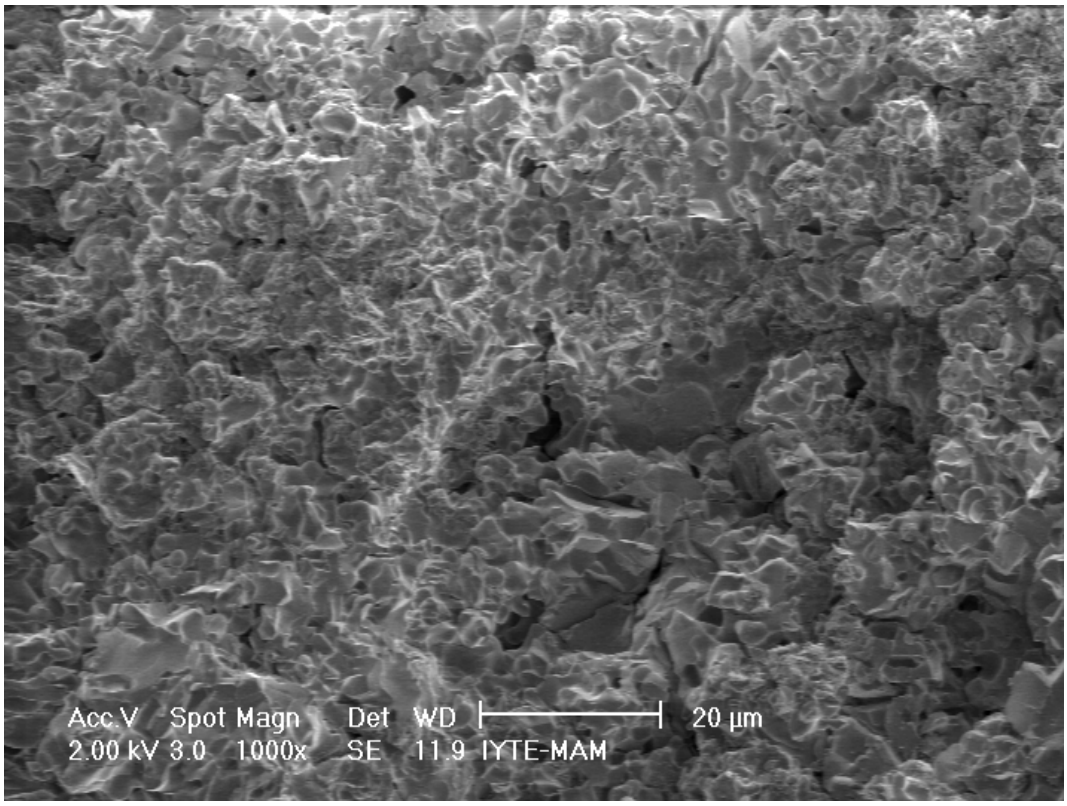

Figure 40. SEM image of 1250 °C sintered composite

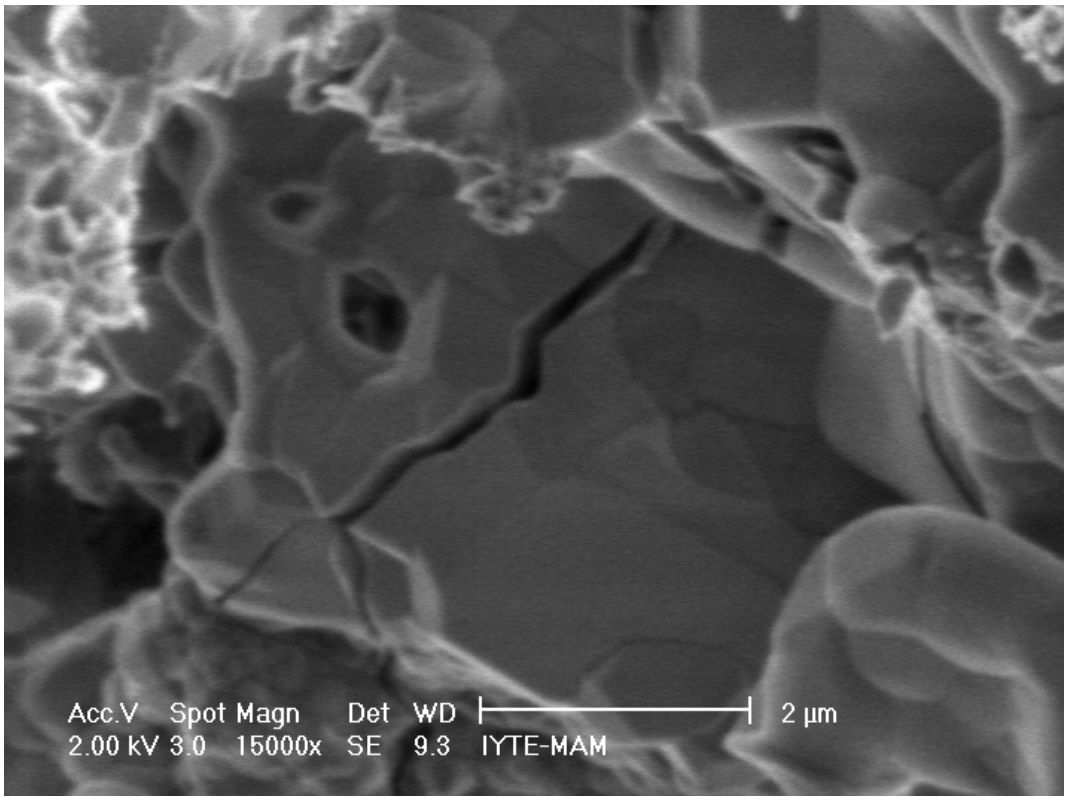

Figure 41. SEM image of 1150 °C sintered composite

5.4. Phase Purity of the Composite

Presence of three ceramic materials with many possible phases formed by transformation or decomposition makes the investigation of phase structure of the composite an important research topic. The reactivity of the three components are considerable at normal conditions and necessitates close examination for optimization of heat treatment temperature at temperatures higher than 1050 °C. The phases that should ideally be present in the material are hydroxyapatite, alumina, and tetragonal yttria stabilized zirconia. Possible phases encountered commonly in literature that may form as a result of reaction between phases at extreme conditions are alpha and beta tricalcium phosphate, tetracalcium phosphate, calcium oxide, calcium aluminate, calcium zirconate, and monoclinic zirconia (Rapacz-Kmita et al. 2004).

Hydroxyapatite decomposes to beta tricalcium phosphate(3), alpha tricalcium phosphate and tetracalcium phosphate(4) at high sintering conditions. These phases are resorbable and tolerated in HA matrix to some extent. But presence of high amounts of these phases results in decreased strength and sinterability of HA.

$$Ca_{10-x}(HPO_4)(PO_4)_{6-x}(OH)_{2-x} \rightarrow Ca_9(PO_4)_6 + (1-x)Ca_{10}(PO_4)_6(OH)_2 \quad (3)$$

$$Ca_{10}(PO_4)_6(OH)_2 \rightarrow Ca_3(PO_4)_6(OH)_2 + Ca_4P_2O_9 + H_2O \quad (4)$$

Hydroxyapatite presence in XRD graphs of composites AZH18, AZH19, AZH20, AZH21, AZH22, AZH23 that have been sintered at 1050 °C indicates that decomposition does not take place at this temperature (Figure 42). Wet mixed composites exhibit a decomposition start temperature at 1200 °C in the presence of more stable pure phases. This may also be valid for composites precipitated with urea precipitation that have less crystalline but functionally isolated phases. It has been reported that thermal stability of hydroxyapatite depends on temperature of precipitation. Hydroxyapatite precipitated at low temperatures with low crystallinity is more prone to decomposition to tricalcium phosphate (Lazic et al. 2001).

It is reported in literature that the influence of zirconia induces faster decomposition of HA (Murugan et al. 2003). To minimize the physical contact between HA and zirconia, alumina layer is aimed to be introduced which has a lower reactivity

with the two phases. Hydroxyapatite reacts with zirconia to form tricalcium phosphate and $CaO\text{-}ZrO_2$ fully stabilized zirconia solid solution by the following reaction:

$$Ca_{10}(PO_4)_6(OH)_2(s) + ZrO_2(s) \rightarrow CaO\text{-}ZrO_2(s) + 3Ca_3(PO_4)_2(s) + H_2O(g) \quad (5)$$

The presence of $CaO\text{-}ZrO_2$ compound is an indication of physical contact between HA and zirconia phases and diffusion of Ca^+ ions to zirconia core. Excessive formation of this phase may result from insufficient coating of alumina in the coated cores. This phase was not seen in the XRD graphs of the composites with beta tricalcium phosphate. This indicates good coating of alumina as a seperator phase and that the presence of beta tricalcium phosphate in sample AZH25 is a result of a deviation in concentrations of calcium and phosphate from stoichiometry at the precipitation stage. This is directly dependent on nucleation and growth mechanisms of Ca^+ and $PO4^-$ ions around nucleation sites on core surfaces that are locally under varying agitation conditions and temperature gradients.

Another phase formation as a result of variations in Ca/P ratio during precipitation stage is monetite or dicalcium phosphate observed in XRD graphs of AZH24 and AZH26. This calcium phosphate is a mineral existing in human dentin and has a Ca/P ratio of 1. It precipitates at a pH less than 5 and temperature around 20°C and can be hydrolysed to hydroxyapatite at pH 10. Its presence may be result of lack of control in pH during precipitation and local variations of temperature in synthesis medium.

Zirconia phase in all composites sintered upto 1250°C remain tetragonal zirconia as seen in the XRD graphs. This had been previously reported for studies on zirconia-hydroxyapatite composites even with presence of decomposed hydroxyapatite that has an accelerating effect on zirconia transformation to cubic zirconia (Guo et al. 2003).

Aluminum-zirconium oxide is a rare impurity observed in AZH22, and AZH23. The reactivity between alumina and zirconia is low and this compound has not been studied in literature. It is a hard and wear resistant phase and its biocompatibility is not well assessed.

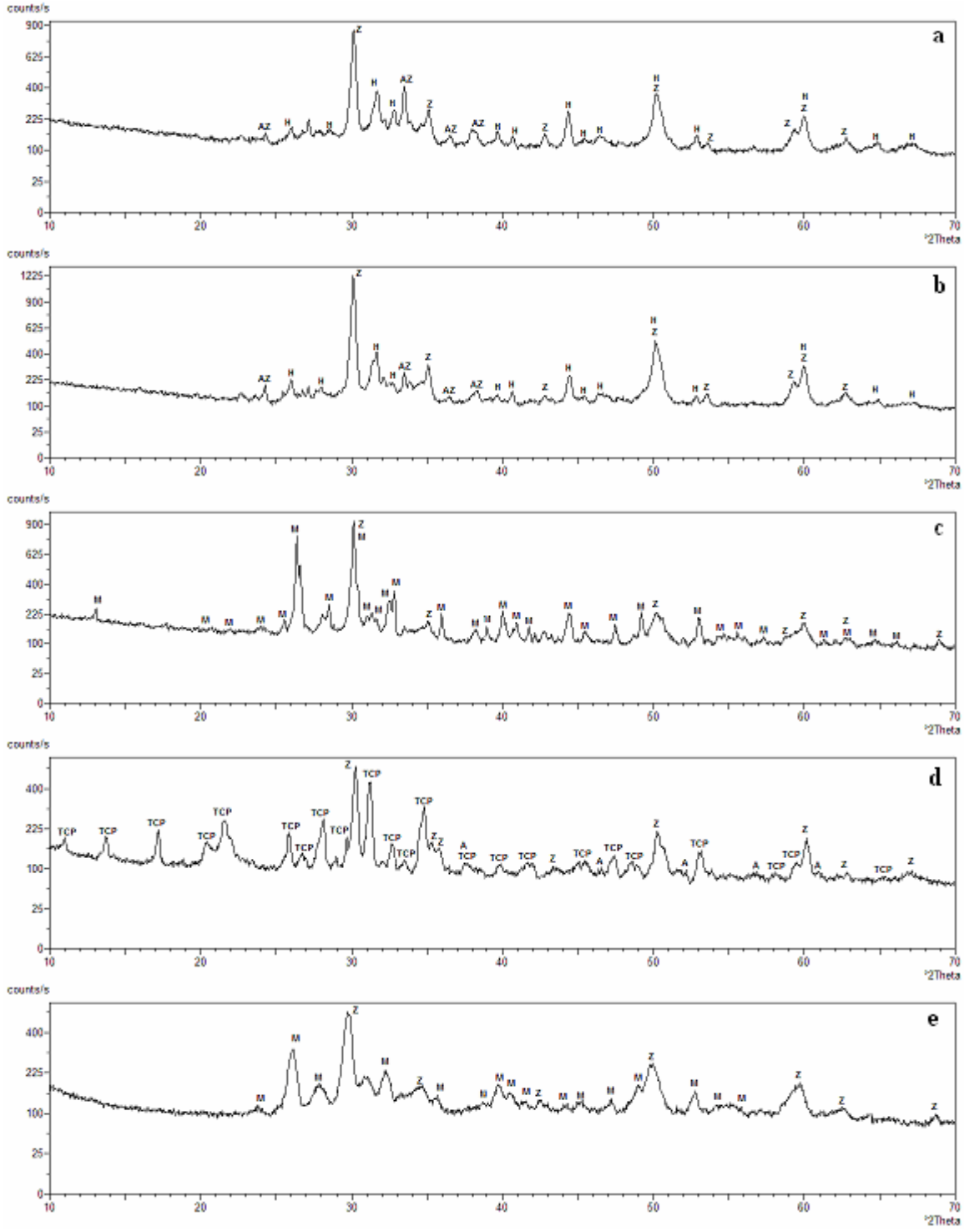

Figure 42. XRD graphs of composites (a)AZH22, (b)AZH23, (c)AZH24, (d)AZH25, (e)AZH26 sintered at 1050 °C (AZ-aluminum zirconium, M-monetitehydroxyapatite, Z-zirconia, TCP-beta tricalcium phosphate)

5.5. Thermal Behavior of the Composite

The sintered AZH18 composite loses nearly 20% of its weight with sintering upto 300°C. This is the amount of adsorbed water released from boehmite and hydroxyapatite in the composite. The two endothermic peaks in the TGA graph shown in Figure 44 indicate two steps of water release. High amount of porosity is formed as a result of gas evolution during sintering upto 300°C which reduces the sinterability of the composite significantly. Similar precipitated hydroxyapatite in the literature provide at most 5 weight percent weight loss so the majority of the water loss is expected from boehmite phase (Lazic et al. 2001). A calcination step prior to sintering is required for improved sinterability of the composite. This is demonstrated by the densifications of 6 samples that have been both directly sintered at 1150 °C and first calcined at 300 °C, pelletized and sintered at 1150 °C in Figure 43. The other endothermic peaks observed in the TGA graph may be associated with the water loss as a result of decomposition reactions (4,5) but α-tricalcium phosphate was not observed in composites sintered upto 1250°C

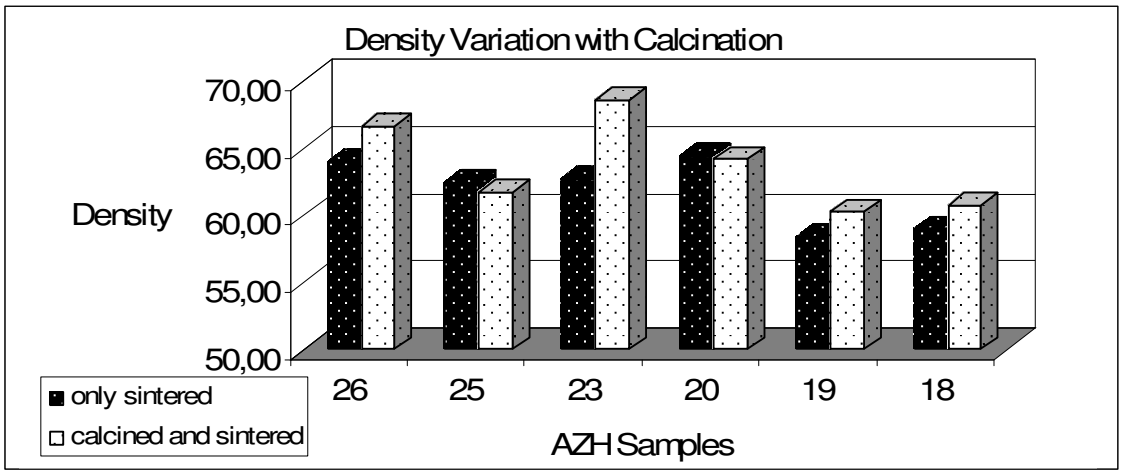

Figure 43. Graph of density variation with calcination of composite samples

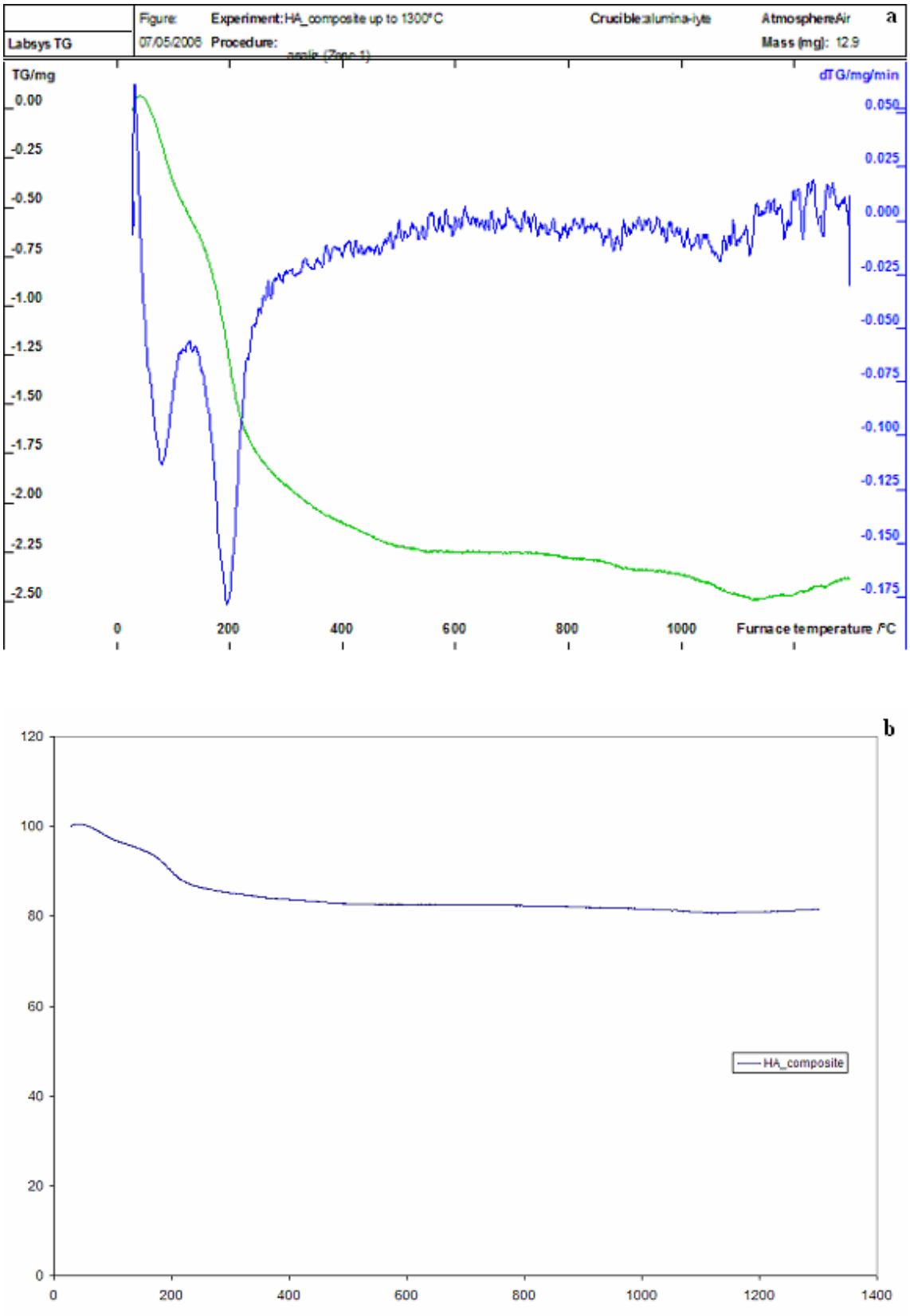

Figure 44. DTA (a) and TGA (b) graphs of the composite sample AZH18

5.6. Mechanical Properties of the Composite

AZH18 has been pressed into pellets of 15 mm diameter and 20 mm length at a pressure of 160MPa using uniaxial pressing machine for determination of compression strength. The pellets have been sintered at three different temperatures of 1050, 1150, 1250 °C to observe the variation of compressive strength with sintering temperature. Compressive stress was applied uniaxially to the pellets with a crosshead speed of 1mm/min. The strength obtained for the three samples are near eachother around 14 MPa without a significant difference with increasing temperature. The stress-strain behavior of the three samples are seen in Figure 45. A reduction in strength near the fracture stress indicates matrix cracking and the sharing of the load by the reinforcement particles of alumina coated zirconia. The micropores in the range of 5-10nm cause stress intensification and intergranular crack propagation as a result of which transformation toughening of embedded zirconia phase does not occur. Strength is expected to increase with increasing densification of the pellets with higher sintering temperature. The sintered densities of the samples are calculated as 1.71 for 1050°C sintered, 1.74 for 1150°C sintered and 1.8 for 1250°C sintered pellets. With increased density the pore size and distribution did not change considerably as seen in the fracture surface images (Figures 38-41) so the stress intensifying effect of the pores and fracture toughness of the composites are expected to be similar for increased sintering temperatures. The compressive strength obtained for AZH18 is higher than compressive strength for cancellous bone which is 12 MPa.

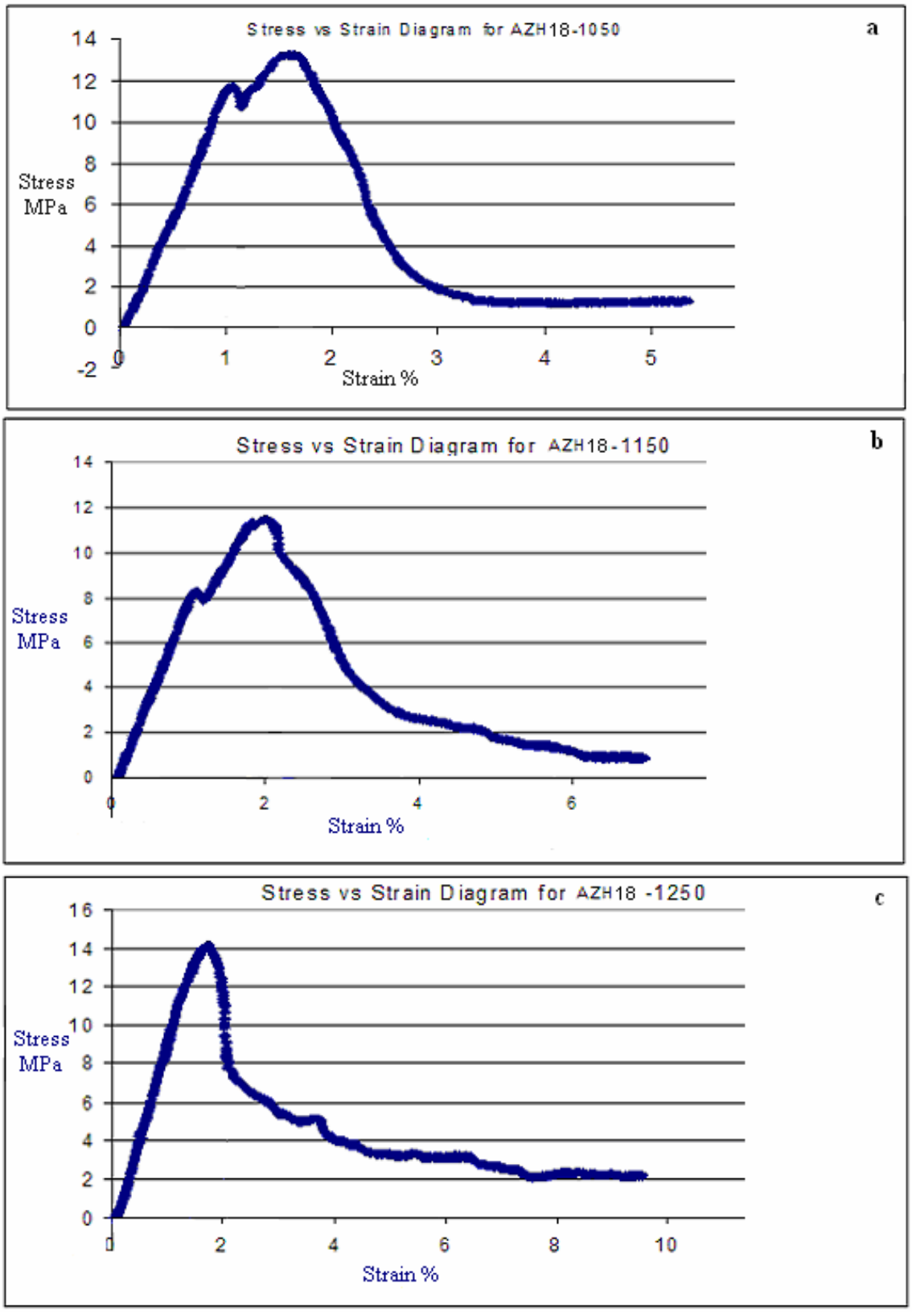

Figure 45. Stress-strain diagrams for AZH18 sintered at (a)1050, (b)1150, (c)1250 °C

CHAPTER 6

CONCLUSION

Synthesis of hydroxyapatite-alumina-zirconia composite is achieved following wet mixing and heterogeneous precipitation route with urea. The wet mixed composites reveal that the sinterability, phase purity and stability of the composite is enhanced with high amount of hydroxyapatite and alumina. 10 volume percent zirconia, 20 volume percent alumina and 70 volume percent hydroxyapatite presents the most suitable composition based on characterizations. The heterogeneous precipitation synthesis process was conducted in two steps; the synthesis of alumina coated yttria stabilized zirconia cores and hydroxyapatite coating the cores. The two processes towards synthesizing uniform 10-20-70 volume percent zirconia-alumina-hydroxyapatite composite powders have been examined for optimization of particle size, particle morphology and phase purity. Precursor stoichiometry, urea/precipitant ratio of 10, homogeneous heating of precipitation medium above 85°C, mild stirring for at least 6 hours, calcination above 300°C prior to sintering, sintering below 1200°C are expected to favour formation of nanoscale composite particles with satisfactory microstructural, thermal stability and mechanical characteristics. Impurity phases observed during synthesis include β-tricalcium phosphate, dicalcium phosphate and aluminum-zirconium oxide. β-tricalcium phosphate and dicalcium phosphate are resorbable apatites tolerated in human bone and dentin. It has been found that alumina effectively eliminates the decomposition reaction between hydroxyapatite and zirconia as an intermediate layer in the particles. The XRD graphs show no trace of $CaZrO_3$ and alpha tricalcium phosphate as decomposition products. Compression strength of the composite of 14MPa has exceeded that of cancellous bone in 50% porous state. Because of presence of micropores lower than 10 micron in size, the matrix can not transfer the load to zirconia phase and transformation toughening does not take place due to intergranular nature of crack propagation. Further mechanical testing is required for the composite consolidated into high density and low density bulk form including fracture toughness, flexural strength tests. The composite is suitable to be processed into porous structure by sponge impregnation or gel casting methods in order to produce a bone-mimetic structure. In vitro bioactivity tests are needed for biocompatibility assesment of the material.

REFERENCES

Aizawa, M., Terado, T., Howell, F.S., Itatani, K., 1998 "Preparation of Spherical Apatite Particles by the Homogeneous Precipitation Method in the Presence of Magnesium Ions and Their Ion Exchange Properties", *Materials Research Bulletin,* Volume 34, Number 8, pp. 1215-1225

Aizawa, M. Ueno, H., Itatani, K., Okada, I., 2006 "Synthesis of calcium-deficient apatite fibres by a homogeneous precipitation method and their characterizations", *Journal of the European Ceramic Society*, Issue 26, pp. 501-507

Balamurugan, A., Balossier, G., Kannan, S., Michel, J., Faure, J., Rajeswari, S., 2006 "Electrochemical and Structural Characterisation of Zirconia Reinforced Hydroxyapatite Bioceramic Sol–gel Coatings on Surgical Grade 316L SS for Biomedical Applications", *Ceramics International,* In Press

Chang, B., Lee, C., Hong, K., Youn, H., Ryu, H., Chung, S., Park, K., 2000 "Osteoconduction at Porous Hydroxyapatite with Various Pore Configurations", *Biomaterials,* Volume 21, Issue 12, pp. 1291-1298

Choi, S. R. and Bansal, N.P., 2005 "Mechanical Behavior of Zirconia/alumina Composites", *Ceramics International,* Issue 31, pp. 39-46

Fu, L., Khor, K.A., Lim, J.P., 2001 "Processing, Microstructure and Mechanical Properties of Yttria Stabilized Zirconia Reinforced Hydroxyapatite Coatings", *Materials Science & Engineering,* Issue 316, pp. 46-51

Giannoudis, P.V., Dinopoulos, H., Tsiridis, E., 2005 "Bone Substitutes: An Update", *Injury, Int. J. Care Injured,* Issue 365, pp. 20-27

Guo, H., 2003 "Laminated and Functionally Graded Hydroxyapatite/Yttria Stabilized Tetragonal Zirconia Composites Fabricated by Spark Plasma Sintering", *Biomaterials,* Volume 24, Issue 4, pp.667-675

Han, Y.H., Park, J.S., 2006 "Effects of MgO coating on microstructure and dielectric properties of $BaTiO_3$", *Journal of the European Ceramic Society*, In Press

Jin, X., 2006 "Martensitic Transformation in Zirconia Containing Ceramics and Its Applications", *Current Opinion in Solid State & Materials Science,* In Press

Jones, R.J. and Hench, L.L., 2003 "Regeneration of Trabecular Bone Using Porous Ceramics", *Current Opinion in Solid State & Materials Science,* Volume 7, pp.301-307

Imai, H., Yamabi, S., 2003 "Synthesis of rutile and anatase films with high surface areas in aqueous solutions containing urea", *Thin Solid Films,* Issue 434, pp.86-93

Katti, K. S., 2004 “Biomaterials in Total Joint Replacement”, *Colloids and Surfaces,* Volume 39, Issue 3, pp.133-142

Kim, H., Kong, Y., Bae, C., Lee, S., Kim, H., 2005 “Improvement in Biocompatibility of ZrO_2-Al_2O_3 Nano-composite by Addition of HA”, *Biomaterials,* Volume 26, Issue 5, pp. 509-517

Kim, H., Kong, Y., Kim, S., Kim, H., 1999 “Reinforcement of Hydroxyapatite Bioceramic by Addition of ZrO_2 Coated with Al_2O_3”, *Journal of American Ceramic Society,* Volume 82, Number 11, pp. 2963-3031

Lazic, S., Zec, S., Miljevic, N., Milonjic, S., 2001 “The Effect of Temperature on the Properties of Hydroxyapatite Precipitated From Calcium Hydroxide and Phosphoric Acid”, *Thermochim.Acta*, Volume 374, Issue 1, pp. 13-22

Mobasherpour, I., Soulati Heshajin, M., Kazemzadeha, A., Zakeri, M., 2006 “Synthesis of Nanocrystalline Hydroxyapatite by Using Precipitation Method”, *Journal of Alloys and Compounds,* In Press

Murugan, R., 2004 “Effect of Zirconia on the Formation of Calcium Phosphate Bioceramics Under Microwave Irradiation”, *Materials Letters,* Volume 58, Issues 1-2, pp. 230-234

Ohtsuka, K., 1991 “Method of Preparing Ceramic Composite Powders and the Powders Obtained Thereby”

Piconi, C., Maccauro, G., 1999 “Zirconia as a Ceramic Biomaterial”, *Biomaterials,* Volume 20, Issue 1, pp. 1-25

Rapacz-Kmita, A., Slosarczyk, A., Paszkiewicz, Z., 2006 “Mechanical Properties of HAp–ZrO_2 Composites”, *Journal of the European Ceramic Society,* Issue 26, pp. 1481-1488

Rapacz-Kmita, A., Slosarczyka, A., Paszkiewicza, Z., Paluszkiewicz, C., 2004 “Phase Stability of Hydroxyapatite–Zirconia (HAp–ZrO_2) Composites for Bone Replacement” *Journal of Molecular Structure,* Issue 704, pp. 333-340

Ratner, B.D., Hoffman, A.S., Schoen, F.J., Lemons, J.E., 2004 “Biomaterials Science, An Introduction to Materials in Medicine, 2nd edition”, (Elsevier Academic Press, San Diego) pp.162

Rosso, M., 2006 “Ceramic and Metal Matrix Composites: Routes and Properties”, *Journal of Materials Processing Technology,* Issue 175, pp. 364-375

Silva, V.V., Lameiras, F.S., Domingues, R.Z., 2001 “Microstructural and Mechanical Study of Zirconia-Hydroxyapatite (ZH) Composite Ceramics for Biomedical Applications” *Composites Science and Technology,* Volume 61, Number 2, pp. 301-310

Stevens, R., 1986 “Zirconia and Zirconia Ceramics, 2nd edition”, (Magnesium Elektron Ltd.)

Suchanek, W. and Yoshimura, M., 1997 “Processing and Properties of Hydroxyapatite-based Biomaterials for Use as Hard Tissue Replacement Implants”, *Journal of Materials Research,* Volume 13, Issue 1, pp.94-117

Taş, C. and Engin, N.O., 1999 “Manufacture of Macroporous Calcium Hydroxyapatite Bioceramics”, *Journal of the European Ceramic Society,* Volume 19, Number 13, pp. 2569-2572

Taş, C., 2004 “Preparation of Porous Bioceramicbsy a Simple PVA Processing Route”, *Key Engineering Materials,* Volumes 264-268, pp. 2079-2082

Vallet-Regi, M., Gonzalez-Calbet, J.M., 2004 “Calcium Phosphates as Substitution of Bone Tissues”, *Progress in Solid State Chemistry,* Volume 32, Issues 1-2, pp. 1-31

Vallet-Regi, M., Ferreira, J.M.F., Rodriguez-Lorenzo, L.M., 2001 “Colloidal Processing of Hydroxyapatite”, *Biomaterials,* Volume 22, Number 13, pp. 1847-1852

Villegas, M., Sierra, T., Caballero, A.C., Fernandez, J.F., 2006 “Ti-based nanocoatings on Al_2O_3 powders”, *Ceramics International*, In Press

Wang, M., 2003 “Developing Bioactive Composite Materials for Tissue Replacement”, *Biomaterials,* Volume 24, Issue 13, pp. 2133-2151

Zhang, M. and Ramay, H.R., 2003 “Preparation of Porous Hydroxyapatite Scaffolds by Combination of the Gel-casting and Polymer Sponge Methods”, *Biomaterials,* Volume 24, Issue 19, pp. 3293-3302